

Breast cancer-on-chip for patient-specific efficacy and safety testing of CAR-T cells

Maulana, T.I.; Teufel, C.; Cipriano, M.; Roosz, J.; Lazarevski, L.; Hil, F.E. van den; ...; Loskill, P.

Citation

Maulana, T. I., Teufel, C., Cipriano, M., Roosz, J., Lazarevski, L., Hil, F. E. van den, ... Loskill, P. (2024). Breast cancer-on-chip for patient-specific efficacy and safety testing of CAR-T cells. *Cell Stem Cell*, *31*(7), 989-1002. doi:10.1016/j.stem.2024.04.018

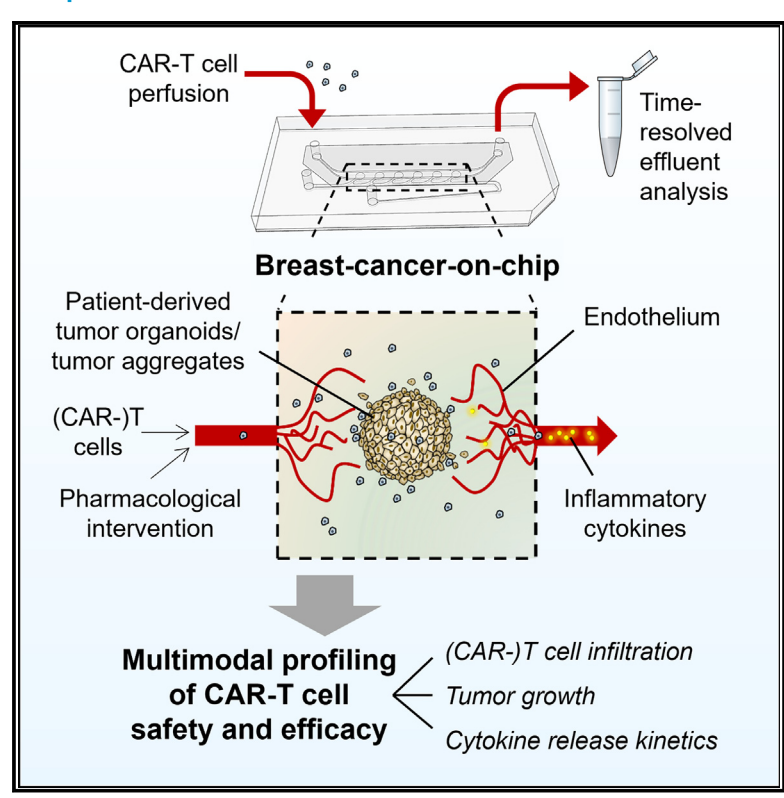
Version: Publisher's Version

License: <u>Creative Commons CC BY 4.0 license</u>
Downloaded from: <u>https://hdl.handle.net/1887/4109100</u>

Note: To cite this publication please use the final published version (if applicable).

Breast cancer-on-chip for patient-specific efficacy and safety testing of CAR-T cells

Graphical abstract



Authors

Tengku Ibrahim Maulana, Claudia Teufel, Madalena Cipriano, ..., Michael Hudecek, Miriam Alb, Peter Loskill

Correspondence

alb_m@ukw.de (M.A.), peter.loskill@uni-tuebingen.de (P.L.)

In brief

Maulana et al. developed an advanced tumor-on-chip model that recreates chimeric antigen receptor (CAR)-T cell infusion, recruitment, and infiltration into solid tumors. Perfused culture enables the monitoring of patient-specific safety and efficacy parameters for over 1 week. The model provides novel opportunities for mechanistic studies of CAR-T cell function in a human-relevant setting.

Highlights

- Tumor-on-chip recapitulating 3D microenvironment with vasculature-like perfusion
- Model for CAR-T cell infusion, recruitment, and infiltration into solid tumors
- Allows for monitoring of dynamic cytokine release over more than 1 week
- Enables in vitro assessment of safety and efficacy in a patient-specific manner







Article

Breast cancer-on-chip for patient-specific efficacy and safety testing of CAR-T cells

Tengku Ibrahim Maulana.^{1,2} Claudia Teufel.¹ Madalena Cipriano.^{1,3} Julia Roosz.² Lisa Lazarevski.¹ Francijna E. van den Hil, 4 Lukas Scheller, 6 Valeria Orlova, 4 André Koch, 5 Michael Hudecek, 6,7 Miriam Alb, 6,8,* and Peter Loskill^{1,2,3,8,9,*}

¹Department of Microphysiological Systems, Institute of Biomedical Engineering, Faculty of Medicine, Eberhard Karls University-Tübingen, 72074 Tübingen, Germany

²NMI Natural and Medical Sciences Institute at the University of Tübingen, 72770 Reutlingen, Germany

SUMMARY

Physiologically relevant human models that recapitulate the challenges of solid tumors and the tumor microenvironment (TME) are highly desired in the chimeric antigen receptor (CAR)-T cell field. We developed a breast cancer-on-chip model with an integrated endothelial barrier that enables the transmigration of perfused immune cells, their infiltration into the tumor, and concomitant monitoring of cytokine release during perfused culture over a period of up to 8 days. Here, we exemplified its use for investigating CAR-T cell efficacy and the ability to control the immune reaction with a pharmacological on/off switch. Additionally, we integrated primary breast cancer organoids to study patient-specific CAR-T cell efficacy. The modular architecture of our tumor-on-chip paves the way for studying the role of other cell types in the TME and thus provides the potential for broad application in bench-to-bedside translation as well as acceleration of the preclinical development of CAR-T cell products.

INTRODUCTION

Chimeric antigen receptor (CAR)-T cells are an innovative cancer immunotherapy that has shown impressive remission rates for the treatment of B cell leukemia and lymphoma and has recently also been approved for the treatment of multiple myeloma. 1,2 The use of this cellular immunotherapy for the treatment of solid tumor entities such as breast cancer has so far been challenging. The main hurdles include the much more heterogeneous expression of relevant target antigens and the physical barriers induced by tumor vasculature and stroma as well as by the abundant presence of immunosuppressive cells and soluble mediators as part of the tumor microenvironment (TME).3,4 Therefore, models that not only incorporate features of the TME but also recapitulate at least partly the three-dimensional (3D) architecture of solid tumors may not only allow to study the efficacy and safety of cancer immunotherapies but may also be able to provide mechanistic insights, e.g., for combinatorial therapy approaches. Additionally, compared with more simplistic twodimensional (2D) coculture assays, these models might also be able to capture interactions of cellular immunotherapies with

the tumor vasculature and other cells within the tumor stroma. Further, incorporation of primary tumor material (e.g., patientderived tumor organoids [PDOs]) may enable studying the efficacy (and safety) of cellular immunotherapies in a patientspecific manner. Such a specific approach is highly desired, as existing (mouse) models often only poorly recapitulate the TME of human tumors as well as the human immune system. 5,6 Moreover, these models are also unsuitable to be implemented in the clinical setting to predict patient response, as their establishment takes months to achieve. Treatment with CAR-T cells and/or other (cellular) immunotherapies can additionally lead to adverse events such as on-target off-tumor effects and may also lead to excessive release of proinflammatory mediators both by the therapeutic as well as bystander (immune) cells.8 Thus, to investigate the mechanisms of adverse reactions and therefore broaden the applicability of this therapy, complex fitfor-purpose in vitro models are needed. Such models should generate results that reflect the human immune system and recapitulate both tumor heterogeneity and the TME; importantly, models with these characteristics should be able to better predict clinical safety and efficacy. Organ-on-chip technologies



³3R Center Tübingen for In Vitro Models and Alternatives to Animal Testing, 72074 Tübingen, Germany

⁴Department of Anatomy and Embryology, Leiden University Medical Center, Leiden 2333 ZA, the Netherlands

⁵Department of Women's Health Tübingen, Eberhard Karls University-Tübingen, 72076 Tübingen, Germany

⁶Medizinische Klinik und Poliklinik II, Lehrstuhl für Zelluläre Immuntherapie, Universitätsklinikum Würzburg, 97078 Würzburg, Germany

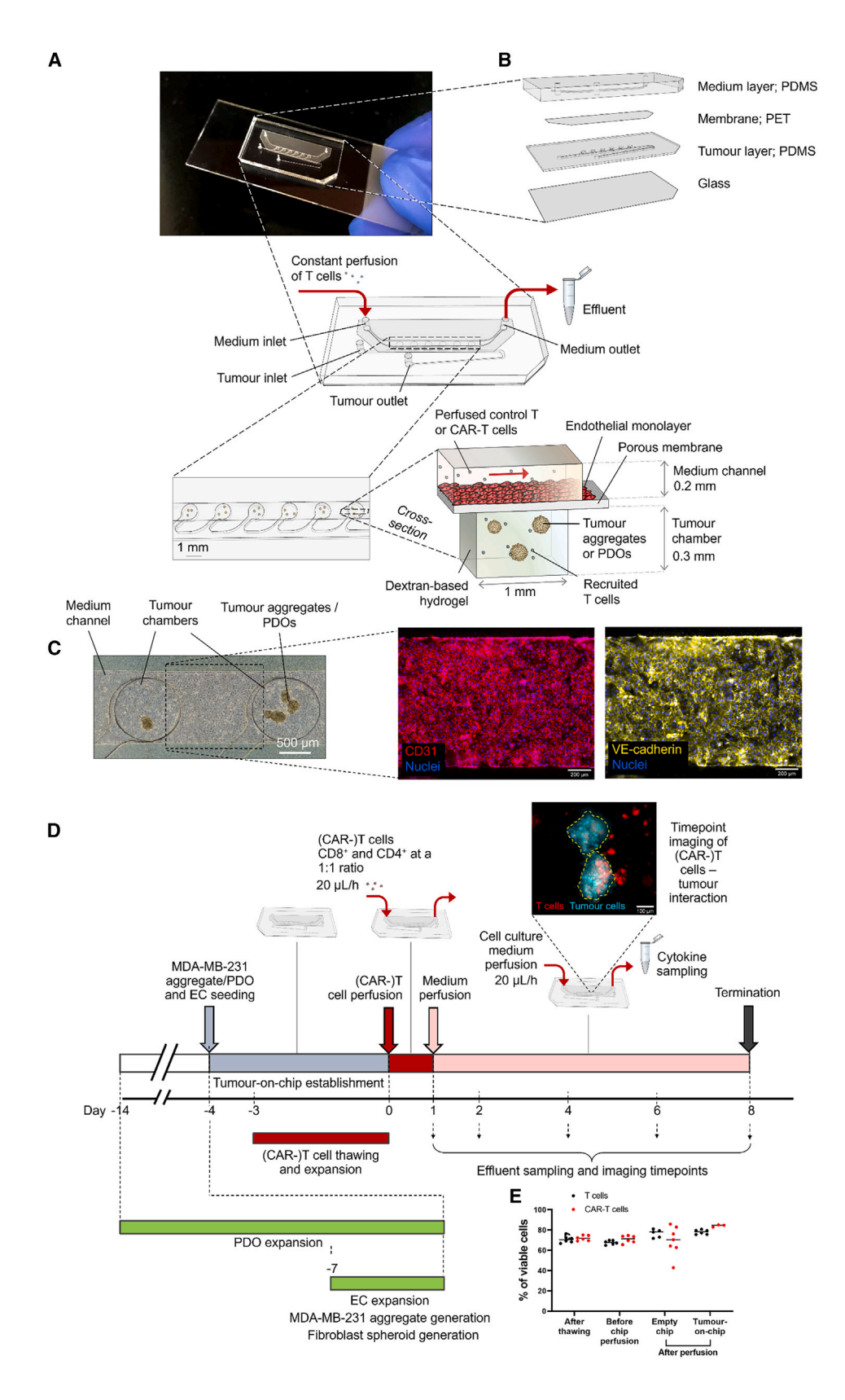
Fraunhofer-Institut für Zelltherapie und Immunologie IZI, Außenstelle Würzburg Zelluläre Immuntherapie, 97082 Würzburg, Germany

⁸These authors contributed equally

⁹Lead contact

^{*}Correspondence: alb_m@ukw.de (M.A.), peter.loskill@uni-tuebingen.de (P.L.) https://doi.org/10.1016/j.stem.2024.04.018







have already demonstrated the potential to fill this translational gap, specifically by recapitulating aspects of the TME⁹ and integrating human immune components. ^{10,11} This type of model can also be established much faster compared with animal models, making it more feasible for direct clinical applications. However, to our knowledge, no organ-on-chip models are currently available to specifically address questions related to CAR-T cell efficacy and safety for patient-specific solid tumors. As part of the imSAVAR project (Immune Safety Avatar; www.imsavar.eu), we develop models to recapitulate the relevant molecular and cellular mechanisms (e.g., key events [KEs] and KE relationships within a specific immune-related adverse outcome pathway [irAOP]) and conditions (e.g., the TME) for an improved prediction of side effects of immunomodulatory therapies.

Here, we introduced a breast cancer-on-chip that recapitulated the initial events occurring upon CAR-T cell administration in patients (CAR-T cell perfusion through the vasculature and extravasation toward the tumor) as well as the effects that manifest over the following week (CAR-T cell infiltration and specific lysis of tumor cells as well as cytokine release [CR]). This enabled us to test varying treatment regimens of dasatinib as a pharmacologic safety switch to control CAR-T cells during the therapy. 12 Lastly, we integrated PDOs with varying receptor tyrosine kinase-like orphan receptor 1 (ROR1) expression levels from metastatic breast cancer patients to demonstrate their applicability in modeling patient-specific effects and revealed a target antigen density-dependent CAR-T cell response. 13 This tumor-on-chip can serve as a standardized, scalable, and explorative platform to evaluate CAR-T cell therapy regarding its efficacy and cytokine-related safety aspects for solid tumors in vitro that may have the potential to predict clinical outcomes.

RESULTS

Tumor-on-chip model with defined vasculature channel enables multi-cell-type tumor tissue generation and immune cell perfusion

To mimic a perfused solid TME, we generated a tumor-on-chip model in which tumor aggregates from a triple-negative breast cancer cell line MDA-MB-231 expressing GFP or PDOs obtained from metastatic breast cancer can be placed on an adjacent endothelialized microchannel (medium channel). Specifically, the tu-

mor aggregates/PDOs were embedded in a dextran-based hydrogel and loaded into six cylindrical tumor chambers (1 mm diameter, 0.3 mm height) that are located underneath a medium channel (0.2 mm height). The medium channel is separated from the tumor chambers by a porous polyethylene terephthalate (PET) membrane (5 µm pore size) and additionally endothelialized to mimic the tumor vasculature (Figure 1A). The MDA-MB-231 cells were aggregated and cultured until they reached \sim 120 μm in size before being loaded into the chip (Figures S1A and S1B). The injection method resulted in approximately 3 tumor aggregates per chamber and 15 per chip, respectively (Figures S1C and S1D). The stacked polydimethylsiloxane (PDMS) channels are microstructured via soft lithography and bottomed with glass to allow high-resolution microscopy (Figure 1B). This arrangement allows for constant (CAR-)T cell perfusion without disturbing the loaded tumor aggregates/PDOs and subsequent (CAR-)T cell migration into the underlying tumor chambers. The perfusion was initiated once a tight endothelial barrier had formed in the medium channel, as indicated by CD31 and vascular endothelial (VE)-cadherin expression as well as barrier permeability for macromolecules (Figures 1C and S3A).

The typical experimental timeline was designed to mimic the first week of CAR-T cell therapy (Figure 1D), as adverse effects such as CR syndrome (CRS) generally occur within the first week after CAR-T cell infusion in patients.8 Following the target cells' injection into the tumor chambers, either primary microvascular (allogeneic)- or human-induced pluripotent stem cell (hiPSC)-derived endothelial cells (ECs) generated from the same (CAR-)T cell donor (isogenic) were seeded into the medium channel and allowed to adhere overnight under static conditions before connecting the chips to constant medium perfusion (20 µL/h) for 1-4 days. All tumor-on-chip systems included ECs unless indicated otherwise. Afterward, the tumor-on-chip systems were perfused with either ROR1-targeting CAR-T cells or untransduced T cells from the same healthy donor as a control (referred to as "control T cells" hereafter). CD19-specific CAR-T cells, generated from the same donor, were used in several experiments as an additional control condition. The (CAR-)T cells were linearly perfused for 20 h with a constant flow rate (20 µL/h), which was followed by cell culture medium perfusion for over 1 week. Here, we first tested perfusion of CAR-T cells at three different concentrations (100,000, 500,000,

Figure 1. Concept and design of the tumor-on-chip and established timeline for CAR-T cell treatment on chip

(A) Schematic representation of the tumor-on-chip model. Tumor aggregates, patient-derived tumor organoids (PDOs), or fibroblast spheroids were embedded in a dextran-based hydrogel and cultured in the cylindrical tumor chambers of the chip, with six chambers in total per chip. The tumor chambers are located underneath a medium channel, which is lined with an endothelial monolayer. Control T cells or CAR-T cells were perfused through the medium channel and can migrate into the tumor chambers.

(B) A magnified view of the individual chip layers and materials. The PDMS medium layer contains the medium channel and the fluid inlets and outlets. The PDMS tumor layer contains the tumor channel and chambers, which are separated from the medium channel by a PET membrane and sealed at the bottom with a glass coverslip to allow high-resolution microscopy.

(C) Brightfield image of two tumor chambers and the medium channel on day 0 before (CAR-)T cell perfusion. The medium channel is covered by a tight monolayer of endothelial cells, as visualized by CD31 and VE-cadherin immunofluorescence staining.

(D) The typical experimental timeline for CAR-T cell efficacy and safety assessment. Target cells—either tumor aggregates, fibroblast spheroids, or PDOs—and endothelial cells were expanded and generated off-chip prior to chip seeding. Cells were seeded and cultured in the tumor-on-chip system for 1–4 days in parallel with the thawing and expansion of control T cells and CAR-T cells. On day 0, either control T cells or CAR-T cells were perfused through the chip for 20 h, followed by medium perfusion. Chips were imaged, and effluents were collected every 1 or 2 days up to day 8.

(E) Viability evaluation via flow cytometry of the control T cells and CAR-T cells after thawing, before, and after chip perfusion (20 h) through empty chip and tumoron-chip setups (collected from the chip effluents); n = 3-7.





and 1,000,000 T cells/mL) while keeping the number of MDA-MB-231 tumor aggregates relatively constant. We selected the values based on the range of peripheral T cell counts in patients who had CRS after receiving CD19-CAR-T cell therapy and proceeded with 500,000 T cells/mL for subsequent experiments, as this concentration, combined with 20 µL/h flow rate setting, produced clinically relevant and detectable cytokine levels (Figure S1E). 14,15 Moreover, concentrations higher than 500,000 T cells/mL often led to T cell clumping in the medium channel, which consequently disrupted the fluid flow. In all experiments, day 0 indicates the starting point of (CAR-)T cell perfusion. The perfusion process and parameters assured 70%-80% T cell viability in both the acellular chip and tumor-on-chip systems (Figure 1E). In summary, we have established an in vitro model, the experimental setup, and the timeline that allows the placement and culture of solid tumor (aggregates/PDOs) near an endothelialized medium channel and the perfusion of (CAR-)T cells without affecting their viability.

CAR-T cells migrate to, infiltrate, and lyse tumoron-chip

To monitor the lytic capacity of CAR-T cells in the tumor-on-chip, the recruitment of control T cells and CAR-T cells was measured in the presence of a microvascular EC (mvEC) barrier. On day 1, both control T cells and CAR-T cells migrated to the GFP-expressing MDA-MB-231 tumor aggregates, with CAR-T cells showing a higher (2.5-fold) fluorescent intensity within the tumor region. Over the 8-day chip culture period, CAR-T cells persisted in/on the tumor aggregates, whereas the control T cells were eventually mostly excluded from tumor aggregates (Figures 2A, 2B, and S2A). Indeed, 3D imaging analysis showed a significantly higher density of infiltrating CAR-T cells (13-fold) within the tumor mass on day 8 when compared with control T cells (Figures 2C and S2B). CAR-T cells were also able to lyse tumor aggregates, as marked by the changes in tumor area and GFP intensity, whereas the tumor aggregates continued to grow in the control T cell condition (Figures 2D and 2E). In addition, on day 8, more dead cells could be observed within the tumor aggregates in the CAR-T cell condition compared with both control T cell and untreated condition (Figure S2C). We observed a higher number of CAR-T cells in the tumor chambers and a stronger tumor growth inhibition both in control T and CAR-T cell conditions when ECs were absent from the system, indicating an inhibitory effect of the endothelium (Figures S3B-S3D). When (CAR-)T cells were perfused at a lower concentration, i.e., 100,000 cells/mL, we observed less (CAR-)T cell infiltration into the tumor aggregates (Figure 2F). However, the number of CAR-T cells that migrated into the tumor chamber remained significantly higher than the number of control T cells. Additionally, at this lower concentration, no (CAR-)T cell migration was observed when no tumor aggregates were present (Figure 2G).

To assess if this CAR-T cell response is target specific, CAR-T cells were perfused through chips containing nonmalignant ROR1⁻ fibroblast spheroids instead of ROR1⁺ MDA-MB-231 tumor aggregates (Figure 2H). Despite migration of the CAR-T cells into the bottom chamber, the fluorescence intensity of CAR-T cells within the fibroblast spheroid region remained low over 1 week compared with that in the MDA-MB-231 aggregates (Figures 2A and 2B). In another set of experiments, we perfused the tumoron-chip models with CD19-specific CAR-T cells, which resulted in a continuous tumor aggregate growth, similar to the control T cell condition (Figure 2E). This demonstrated ROR1-specific CAR-T cell reactivity and the utility of the model for evaluating possible off-target effects by integrating cells from nonmalignant

Assessment of CAR-T cell CR kinetics in the tumor-onchip model

In patients, CAR-T cell therapy is often accompanied by increased proinflammatory cytokine levels in the peripheral blood (including interleukin 6 [IL-6]), which may induce CRS. In such cases, patients can be treated with multiple doses of IL-6 receptor-blocking antibodies and/or glucocorticoids or even vasopressors in cases of higher-grade CRS. 16 The molecular and cellular steps that may result in CRS can be described using the AOP concept, which is widely used in immunotoxicology. 17 Within the EU project imSA-VAR, we established an irAOP describing the key molecular and cellular events that lead to CRS mediated by CAR-T cells. To model the early KEs of this irAOP, in particular KE1 (activation/proliferation of CAR-T cells, release of proinflammatory mediators), 18 and monitor the levels of clinically relevant (pro)inflammatory cytokines in the tumor-on-chip, we initially tested whether the cytokines originate from the CAR-T cell-tumor interaction. Here, we perfused either CAR-T cells or control T cells through acellular (empty), EC barrier (mvECs) only, or complete tumor-on-chip models, which included both mvECs and MDA-MB-231 tumor aggregates. We ensured that the mvECs expressed no ROR1 to exclude on-target off-tumor effects (Figure S1F). Compared with those in the control T cell condition, the levels of nearly all quantified cytokines-namely IL-2, IL-6, tumor necrosis factor alpha (TNF- α), interferon gamma (IFN- γ), and serine protease granzyme B-were higher (ranging from 6- to 100-fold) in the CAR-T cell condition on day 1 when tumor aggregates were present, whereas the level of anti-inflammatory cytokine IL-10 remained low in all conditions. The cytokine levels remained relatively lower in conditions without tumor aggregates, showing that cytokine secretion was mainly induced by target antigen recognition (Figure 3A).

In patients, however, CRS onset occurs beyond 1 day and develops over multiple days.8 Understanding the effect of potential mitigation strategies to manage the release kinetics of proinflammatory mediators and investigate the role of different cell types in perpetuating this proinflammatory cycle therefore requires a model that is viable and functional for this specific period. Here, linear perfusion of the CAR-T cell-treated tumor-on-chip allows such "real-time" monitoring of the cytokine level by measuring it on the chip effluents. By assessing tumor-on-chip perfused culture for up to day 8, our data showed that the peak cytokine concentration in the CAR-T cell condition occurred on either day 1 or 2 for all measured cytokines listed above. Cytokine concentrations in the CAR-T cell condition were consistently higher than those in the control T cell condition at almost all measured time points (Figure 3B). Moreover, both the perfusion of ROR1-CAR-T cells in chips containing ROR1 fibroblast spheroids and CD19-CAR-T cells in chips containing ROR1⁺ MDA-MB-231 tumor aggregates resulted in lower cytokine levels compared with ROR1-CAR-T cells and ROR1+ MDA-MB-231 combination at most time points, showing a target-dependent cytokine response (Figures S4A and S4B).



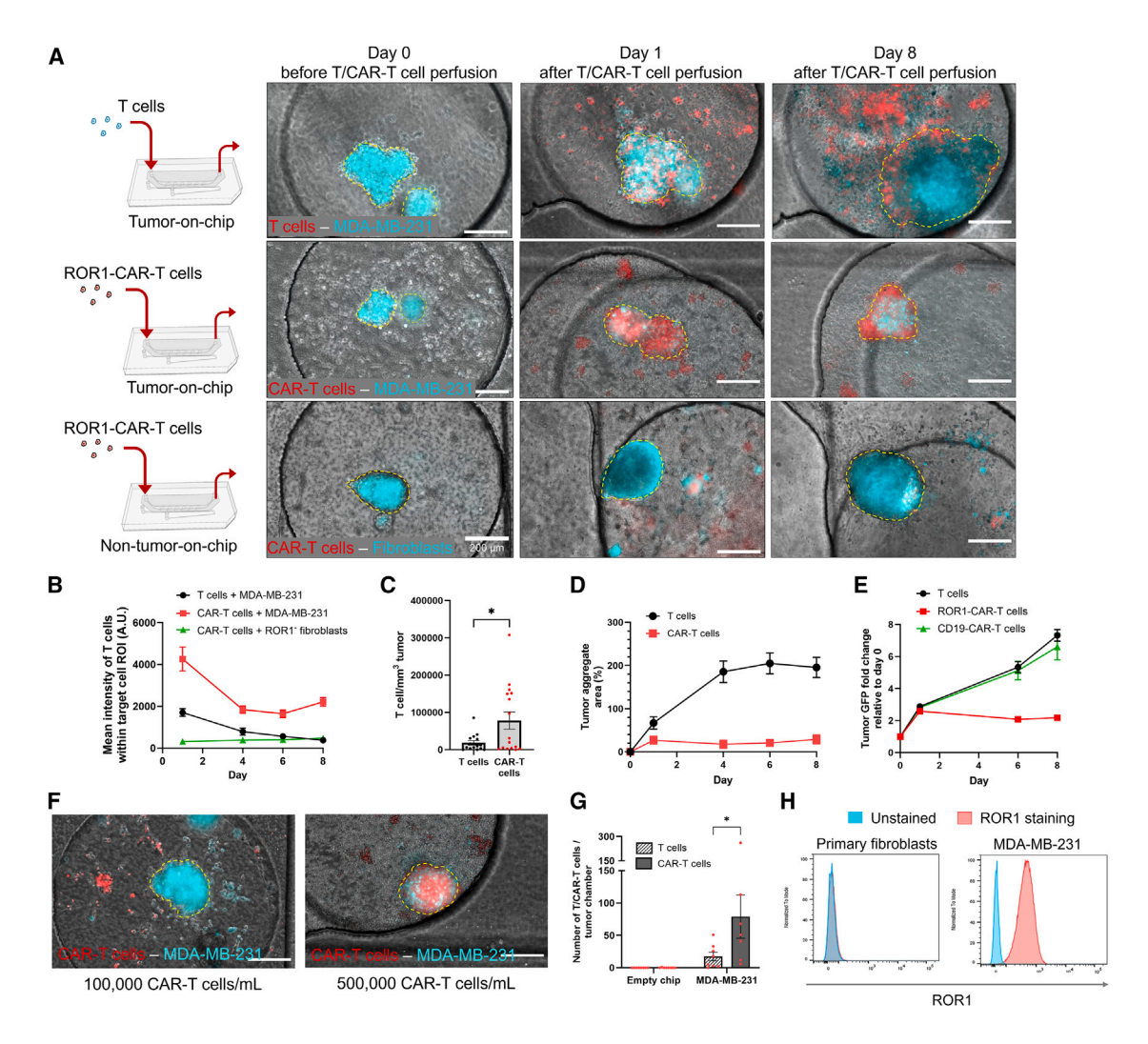


Figure 2. CAR-T cells infiltrated the tumor aggregates and hampered their growth in a target-specific manner on chip

(A) Representative images of MDA-MB-231 aggregates or fibroblast spheroids on day 0 (before [CAR-]T cell treatment), and on days 1 and 8 after tumor-on-chip perfusion with control T cells or CAR-T cells. MDA-MB-231 tumor cells express GFP and are pseudocolored cyan. Fibroblasts—representing nonmalignant tissue as a control—were labeled with CellTracker 5-chloromethylfluorescein diacetate (CMFDA) and pseudocolored cyan. Control T cells and CAR-T cells were labeled with CellTracker deep red. The yellow dashed line marks the region of interest of each tumor aggregate or fibroblast spheroid. MvECs were present in all chips. Scale bars, 200 μm.

- (B) Quantification of the mean intensity values of the control T cells and CAR-T cells within each tumor aggregate or fibroblast spheroid region of interest at different time points after (CAR-)T cell perfusion; n = 7–21 MDA-MB-231 tumor aggregates/fibroblast spheroids from 3–4 chips. Data are presented as the mean \pm SEM.
- (C) Quantification of infiltrating (CAR-)T cells per mm³ of tumor volume on day 8 after (CAR-)T cell treatment; n = 15-16 MDA-MB-231 tumor aggregates from 3 chips. Data presented as the mean \pm SEM. *p < 0.05; two-tailed unpaired t test.
- (D) MDA-MB-231 tumor aggregate growth after CAR-T cell treatment in comparison with (control) T cell treatment, as measured by quantifying the percentage change in each MDA-MB-231 aggregate area between certain time points and the initial area before (CAR-)T cell perfusion; n = 12–16 aggregates from 4 chips. Data are presented as the mean ± SEM.
- (E) Quantification of the fold change in the mean GFP intensity of MDA-MB-231 tumor aggregates in each tumor chamber on days 1–8 after the perfusion of (control) T cells, ROR1-CAR-T cells, or CD19-CAR-T cells relative to day 0; n = 24 tumor chambers from 4 chips. Data are presented as the mean \pm SEM.
- (F) Representative images on day 1 after perfusing CAR-T cells (red) through the tumor-on-chip setup containing MDA-MB-231 aggregates (cyan), with a CAR-T cell concentration of either 100,000 or 500,000 cells/mL. The focal plane was set on the aggregates for all acquisitions. Scale bars, 200 µm.
- (G) Quantification of control T cells or CAR-T cells per tumor chamber on day 1 after the tumor-on-chip was perfused at a concentration of 100,000 (CAR-)T cells/ mL. An empty chip was used as a control; n = 7-8 chambers from 3 chips. Data are presented as the mean \pm SEM. *p < 0.05; Bonferroni's multiple comparisons test.
- (H) Flow cytometry histograms showing ROR1 expression (red) in MDA-MB-231 cells and fibroblasts compared with the unstained control (cyan). See also Figures S2 and S3.



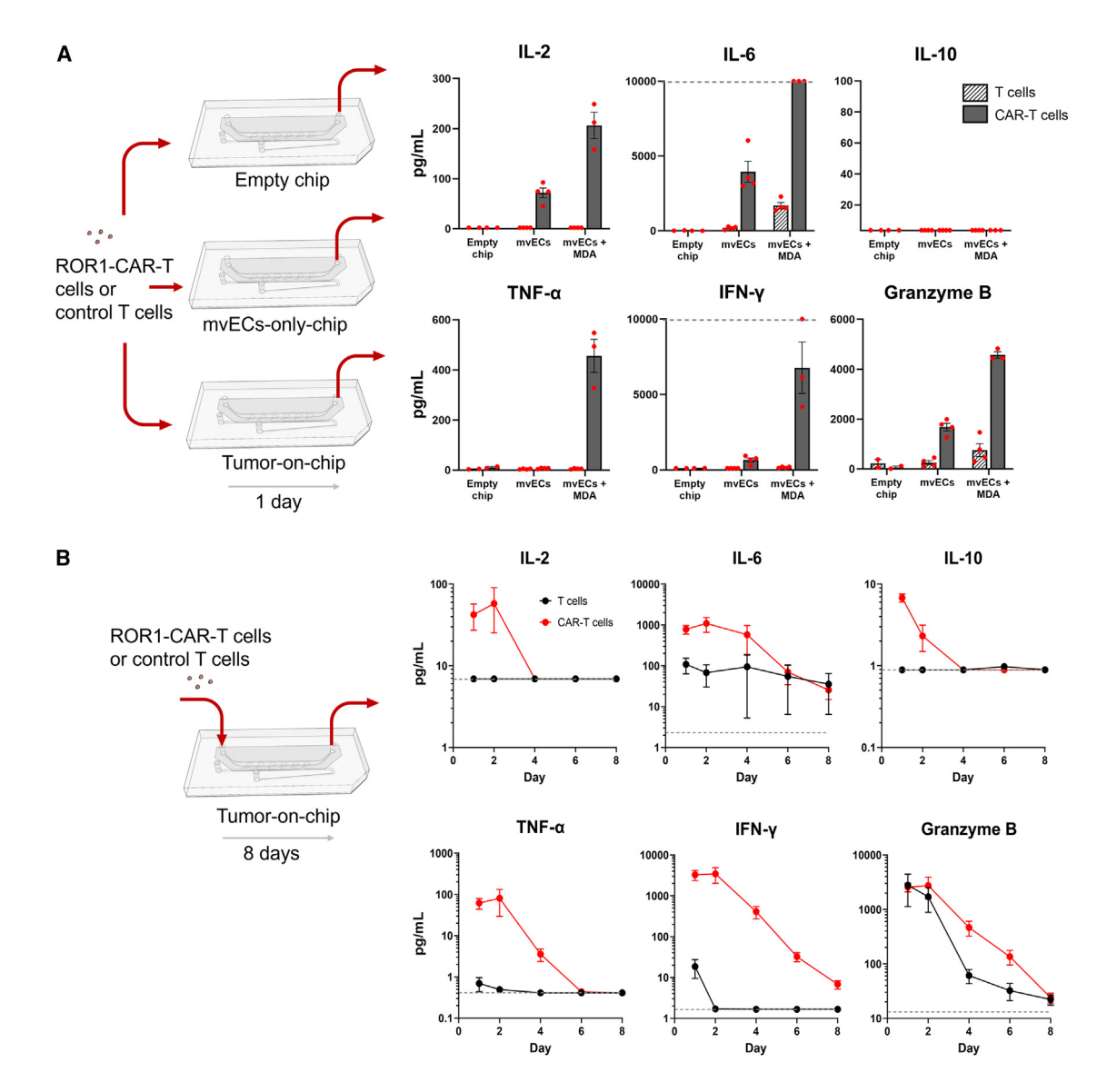


Figure 3. CAR-T cell-mediated cytokine concentrations and release kinetics in the tumor-on-chip model

(A) CAR-T cell-treated tumor-on-chip systems were assessed with regards to the secretion of cytokines IL-2, IL-6, IL-10, TNF- α , IFN- γ , and granzyme B on day 1 (20 h) after CAR-T cell perfusion. To ensure that the cytokines originate from CAR-T cell-tumor interaction, either control T cells or CAR-T cells were perfused through either acellular (empty), mvEC-only, or complete tumor-on-chip setups (mvECs + MDA); n = 2-4 chips. Data are presented as the mean \pm SEM. Each red dot represents one chip. The dashed line indicates the upper detection limit.

(B) Release kinetics of the abovementioned cytokines from days 1 to 8 after control T cell or CAR-T cell perfusion from days 0 to 1. Samples were collected every 1-2 days; n = 4 chips. Data are presented as the mean ± SEM. The dashed line indicates the lower limit of detection. See also Figure S4.

By using this setup, we were able to recapitulate clinically relevant cytokine levels and kinetics, mimicking the initial surge in inflammatory cytokine secretion at the tumor site that was induced by target antigen recognition, which could induce CRS in patients undergoing CAR-T cell therapy.

On/off functional control of CAR-T cells in the tumor-onchip model

As clinical CR kinetics were successfully mimicked using the CAR-T cell-treated breast cancer-on-chip models, we next tested whether the CR kinetics could be pharmacologically altered to model therapeutic intervention and prevention of CRS onset. The occurrence of CRS is very challenging to predict, 19 and modeling release kinetic of key CRS mediators requires a tailored human-relevant setup that includes relevant cell types in a perfused microenvironment. Once it occurs, a pharmacological intervention that enables a temporary "pause" in CAR-T cell activity upon the onset of this immune-related adverse event could save patients from severe adverse reactions. 20 Dasatinib is a Food and Drug Administration (FDA)-approved tyrosine kinase inhibitor that reversibly inhibits the phosphorylation of CD3 ζ and ζ -chain of T cell receptor-associated protein kinase 70 (ZAP70) in CAR constructs

Article



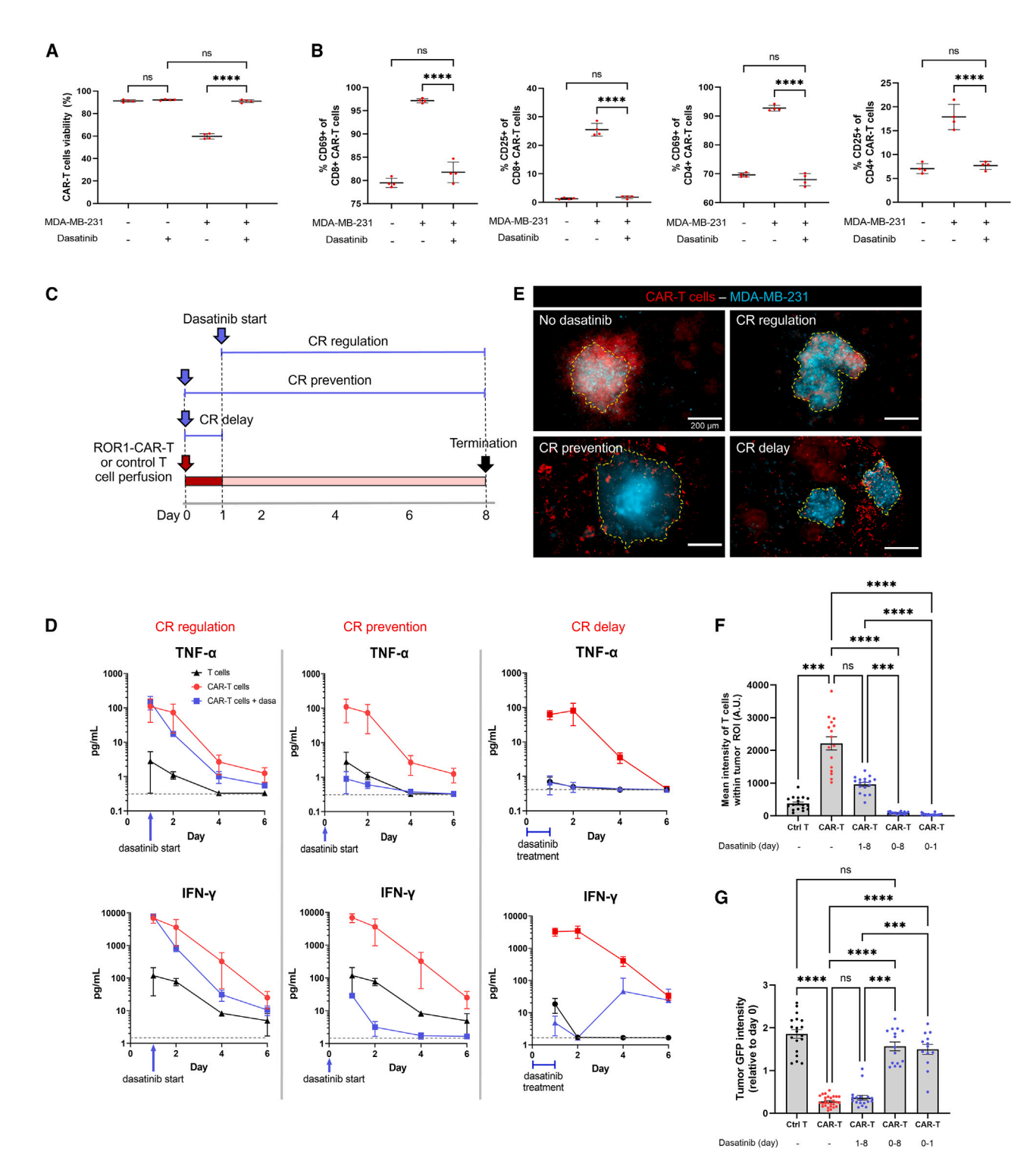


Figure 4. Dasatinib treatment regimens to model intervention strategies on CAR-T cell-treated tumor-on-chip models

(A) CAR-T cell viability after 24 h of dasatinib (50 nM) treatment either in the presence of MDA-MB-231 cells (effector-to-target cell ratio, 10:1) or without, cultured

(B) Percentage of CD69+ (early activation) and CD25+ (late activation) CAR-T cells within the CD8+ and CD4+ subset after 24 h of dasatinib (50 nM) treatment either in the presence of MDA-MB-231 cells (effector-to-target cell ratio, 10:1) or without, cultured in a well-plate format. Data were acquired from flow cytometry analysis for both (A) and (B); n = 4 wells. Data are depicted as mean with \pm SEM. Each red dot represents one well. ns, not significant, ****p < 0.0001; Tukey's multiple comparisons test.





containing either CD28 CD3 cor 4-1BB CD3 cactivation modules. In experiments using cell culture plates, we initially confirmed that dasatinib (50 nM) did not negatively affect CAR-T cell viability and successfully inhibited the upregulation of early (CD69) and late (CD25) activation markers after 24 h of interaction with MDA-MB-231 cells (Figures 4A and 4B). Afterward, we quantified the effects of dasatinib that was applied either throughout the CAR-T cell treatment period on the tumor-on-chip models (days 0-8; CR prevention regimen), before the peak of cytokine secretion (days 0-1; CR delay regimen), or after the peak of cytokine secretion (days 1-8; CR regulation regimen) (Figure 4C).

Applying dasatinib after the peak of cytokine secretion (days 1–8; CR regulation) resulted in a rapid drop in TNF- α and IFN- γ levels relative to those in the untreated CAR-T cell condition (Figure 4D), thereby mimicking acute management of early release of CRS mediators.²¹ This treatment scheme also enabled infiltration of CAR-T cells into the tumor within the first 24 h (before dasatinib treatment) but not subsequent excessive infiltration, as indicated by the lower fluorescence intensity (~2-fold) compared with that in the untreated CAR-T cell condition (Figures 4E and 4F). Furthermore, the tumor GFP signal intensity on day 8 dropped to a level similar to that observed in the CAR-T cell condition without dasatinib (Figure 4G), indicating the maintenance of the baseline level of antitumor cytotoxicity.

Dasatinib administration throughout the CAR-T cell treatment period (days 0-8; CR prevention) prevented the CR, as shown by the lower TNF- α and IFN- γ levels compared with those observed with untreated CAR-T cells and control T cells (Figure 4D). However, this treatment scheme also prevented CAR-T cells from infiltrating the tumor, and the signal intensity in the GFP-expressing MDA-MB-231 tumor aggregates changed only minimally, with no significant difference compared with that in the control T cell condition (Figures 4F and 4G). Therefore, this approach defeats the purpose of CAR-T cell treatment. The day 0-1 treatment approach delayed the IFN- γ peak but not the TNF- α peak, revealing the transient effect of dasatinib (Figure 4D). However. this approach also prevented CAR-T cells from infiltrating and lysing the tumor aggregates as seen on day 8 (Figures 4E-4G).

By investigating different intervention time points and durations using dasatinib in the tumor-on-chip models, we demonstrated the feasibility of the model to investigate a suitable intervention strategy by controlling the secretion of CAR-T-cell-derived CRS mediators without diminishing CAR-T cell efficacy.

PDOs on chip demonstrate antigen-dependent, potent antitumor efficacy of ROR1 CAR-T cells

ROR1 expression levels are tumor and patient specific. 22,23 To evaluate therapeutic efficacy within the context of this heterogeneity, we integrated PDOs derived from two female patients with metastatic breast cancer that had high or low ROR1 levels (Figure 5A; Table S1) and compared them with MDA-MB-231 aggregates as a positive control condition. To evaluate tumor- and patient-specific effects of the PDOs, possible alloreactive responses of T cells toward ECs-e.g., when primary allogeneic mvECs were employed—were excluded by integrating hiPSCderived ECs sourced from the same donor as the (CAR-)T cells.

In the semiautologous tumor-on-chip setup, CAR-T cell infiltration into the PDOs (Figures 5B-5D), PDOs' growth (Figure 5E), cytokine secretion (Figures 5F and S5D), and release kinetics (Figure 5G) varied according to ROR1 expression of the PDOs. Consistent with the respective target expression levels, CAR-T cells infiltrated ROR1-high PDOs in significantly higher numbers (9-fold) than ROR1-low PDOs. The highest CAR-T cell infiltration rate was observed in MDA-MB-231 aggregates, with an infiltration rate 2-fold higher than that in ROR1-high PDOs (Figure 5C). Additionally, ROR1-low PDOs continued to grow despite CAR-T cell treatment, whereas the growth of ROR1-high PDOs was restricted (Figures 5D and 5E). In another set of experiments, we integrated PDOs derived from two additional female patients and observed a similar trend (Figures S5A-S5C; Table S1).

Notably, despite the absence of CAR, control T cells were still recruited into the tumor chamber, which might indicate a baseline allogeneic response toward the PDOs. However, control T cells mostly remained excluded from the PDOs after the culture period (Figure 5B) and exhibited much lower cytokine levels on day 1 than the respective CAR-T cell condition (Figure 5F). In summary, our results indicate that the tumor-on-chip can also capture a patient-specific response by integrating tumor target cells obtained directly from patients to assess both the efficacy and CRS-related safety aspects.

DISCUSSION

This breast cancer-on-chip demonstrates the feasibility to evaluate the efficacy (T cell infiltration, tumor growth, and lysis), safety (abundant CR that could lead to CRS), as well as CR intervention strategies of CAR-T cell therapy for solid tumors in vitro. We

⁽C) Timeline of dasatinib treatment regimens with varying starting time points (blue arrows) and durations (blue bar lengths) during tumor-on-chip culture to control the release of CRS mediators. Tumor-on-chip systems containing MDA-MB-231 aggregates were perfused on days 0-1 with either control T cells or CAR-T cells and then with cell culture medium from days 1-8. Dasatinib (50 nM) was administered through the tumor-on-chip models on days 1-8, 0-8, or 0-1 to model cytokine release (CR) regulation, prevention, or delay, respectively.

⁽D) TNF-α and IFN-γ release kinetics in the control T cell, CAR-T cell, and CAR-T cell + dasatinib conditions with three different treatment schemes: CR regulation (left), prevention (middle), and delay (right). Cytokines were measured from the tumor-on-chip effluents. Data are shown as the mean ± SEM. The dashed line indicates the lower limit of detection. Data points from day 8 are excluded as the values are mostly below the detection limit, n = 4 chips per condition.

⁽E) Representative images of MDA-MB-231 aggregates (cyan) on day 8 after tumor-on-chip perfusion with CAR-T cells (red), showing different degrees of T cell infiltration into the aggregate after applying different dasatinib treatment schemes compared with an image of untreated cells. Conditions are indicated at the top left of each image. The yellow dashed line marks the region of interest of one tumor aggregate. Scale bars, 200 µm.

⁽F) Quantification of the mean intensity values of the control (Ctrl) T cells and CAR-T cells within each MDA-MB-231 tumor aggregate region on day 8 after or without dasatinib treatment; n = 15-18 MDA-MB-231 aggregates from 3-4 chips. Data are presented as the mean ± SEM. ns, not significant, ***p < 0.001, ****p < 0.0001; Dunn's multiple comparisons test.

⁽G) Quantification of the fold change in the mean GFP intensity for each MDA-MB-231 tumor aggregate on day 8 relative to the mean GFP intensities of the aggregates on day 0 to assess tumor lysis. Each dot represents one MDA-MB-231 aggregate. Data are shown as the mean ± SEM; n = 13-28 aggregates from 3-4 chips. ns, not significant, ***p < 0.001, ****p < 0.0001; Dunn's multiple comparisons test.



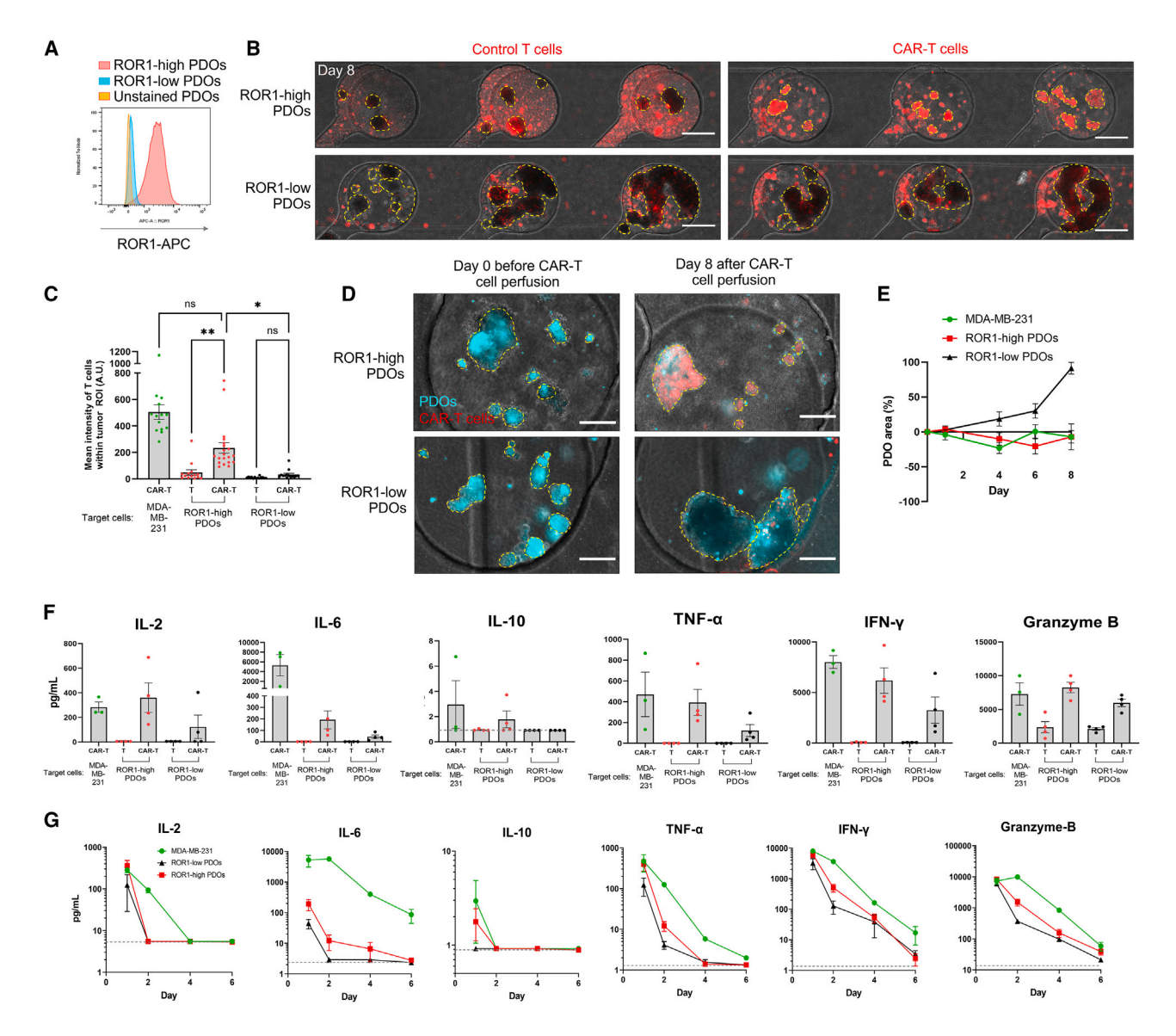


Figure 5. CAR-T cell infiltration, cytokine secretion, and tumor growth restriction depend on ROR1 expression of the patient-derived tumor organoids

(A) Flow cytometry histogram plots showing ROR1 expression in high-ROR1-expressing patient-derived tumor organoids (PDOs) (red) and low-ROR1-expressing PDOs (cyan) from patients with metastatic breast cancer compared with the unstained control (orange).

(B) Representative images of ROR1-low and ROR1-high PDOs on day 8 after perfusion with either control T cells or CAR-T cells (red). PDOs are marked with yellow dashed line. Scale bars, $500 \mu m$.

(C) Quantification of the mean intensity values of the control T cells (notated as "T" in the x axis labels) and CAR-T cells within the region of interest of each PDO on day 8. MDA-MB-231 aggregates were used as a positive control; n = 14-20 PDOs from 3-4 chips. Data are presented as the mean \pm SEM. ns, not significant, $^*p < 0.05$, $^{**}p < 0.01$; Dunn's multiple comparisons test.

(D) Representative images of ROR1-high and ROR1-low PDOs (cyan) before CAR-T cell (red) perfusion and on day 8 of the experiment. The yellow dashed line marks the region of interest of the PDOs. Scale bars, 200 µm.

(E) PDO growth after CAR-T cell treatment, as measured by quantifying the percentage change in PDO area in each tumor chamber at certain time points relative to the initial area before CAR-T cell perfusion. MDA-MB-231 aggregates were used as a positive control; n = 18–24 tumor chambers from 3–4 chips. Data are presented as the mean ± SEM.

(F) Quantification of IL-2, IL-6, IL-10, TNF- α , IFN- γ , and granzyme B levels in the effluents of the chips after 20 h of control T cell or CAR-T cell perfusion through the tumor-on-chip systems containing MDA-MB-231 aggregates (positive control for CAR-T cell treatment), ROR1-high PDOs, or ROR1-low PDOs; n = 3-4 chips. Data are presented as the mean \pm SEM. Each red dot represents one chip.

(G) Cytokine release kinetics of the abovementioned cytokines from days 1 to 6 after CAR-T cell perfusion from days 0 to 1 through the tumor-on-chip setups containing MDA-MB-231 aggregates (positive control for CAR-T cell treatment), ROR1-high PDOs, or ROR1-low PDOs; n = 3-4 chips. Data are presented as the mean \pm SEM. The dashed line indicates the lower limit of detection. Data points from day 8 are excluded as the values are mostly below the detection limit. See also Figures S3 and S5 and Table S1.





demonstrated the feasibility and power of modeling aspects of early KEs at the tumor site upon therapy administration in a physiologically relevant coculture model and applied clinically relevant readouts. Bottom-up approach in designing the tumor microarchitecture, perfusion setup, and modularity in cellular and microenvironmental components allowed us to adjust the model complexity and exclude off-target effects while ensuring human and clinical relevance, thereby addressing several limitations of existing model systems to evaluate CAR-T cell performance.

First, our data showed that the tumor-on-chip successfully captured differences in T cell infiltration into the tumor, tumor growth, and cytokine response that depended on CAR expression on engineered T cells and ROR1 expression on the target cells during 8 days of perfused tumor-on-chip culture. By perfusing CAR-T cells or control unmodified T cells through the blood vessel-like channel, we could assess their recruitment to the tumor site and observed that CAR-T cells infiltrated the MDA-MB-231 aggregates at a higher density and persisted longer than control T cells. We observed the exclusion of unmodified control T cells from the tumor aggregates after 1 week of culture-a clinical phenomenon reported to predict the subset of cancer patients who are not responsive to cancer immunotherapy.^{24,25} Moreover, including ECs in the tumor-on-chip resulted in fewer recruited CAR-T cells in the tumor chamber and reduced tumor growth control (Figures S3B-S3D). The vasculature of tumors indeed poses a barrier for T cell trafficking, which has long been proposed as a therapeutic target in cancer immunotherapy.^{26,27} Future studies using tumor-on-chip or similar models could investigate strategies to overcome this inhibitory effect of the tumor vasculature and therefore improve CAR-T cell homing into the tumor. Moreover, such inhibitory effects of the TME could be underestimated in the well-plate setting, as we saw a significantly higher T cell and CAR-T cell infiltration and lower tumor GFP intensity values on day 1 compared with those in the chip setup (Figures S2D and S2E).

Furthermore, the ability to integrate the PDOs directly from patients and establish the tumor-on-chip model faster compared with murine models (in a week instead of several months) may allow for utilizing the model to assist clinical decision-making, which often requires a short time scale. In our setup, we found that relative ROR1 expression on PDOs positively correlated with the persistence of CAR-T cells within the tumor bulk, which aligned with recently published data showing that the antitumor killing of breast tumor-derived PDOs within the first 24 h positively correlates with the ROR1 expression level.²⁸ Integrating patient-specific PDOs in our system helps to reconstitute the TME surrounding the PDOs and therefore the physiological relevance, thereby improving existing in vitro models with PDOs that focused mainly on assessing treatment efficacy.^{28–33}

Next, we observed abundant release of proinflammatory cytokines in our models, which allowed us to study intervention strategies using dasatinib as a functional on/off switch of CAR-T cells. On either day 1 or 2 of CAR-T cell administration, we consistently detected peaks in cytokine levels. Cytokine levels typically decreased afterward, but whether this was caused by activation-induced T cell death following eradication of the tumor cells or T cell exhaustion remains to be investigated. This drop of cytokine levels might also result from the ongoing lysis of MDA-MB-231 tumor aggregates by the CAR-T cells, as the tumors stopped growing in this condition, as shown in previous efficacy test runs. Additionally, replacing the non-recruited CAR-T cells with cell culture medium in the perfusate from day 1 may limit cytokine secretion from only the recruited CAR-T cells on subsequent days. Nevertheless, the presence of granzyme B was still detected on day 8 of culture in both the CAR-T cell and control T cell conditions, indicating an ongoing T cell-tumor interaction. Early secretion—up to day 3 after CAR-T cell administration—of IFN-γ was shown to predict the development of severe CRS.³⁴ Circulating IFN-γ levels have been associated with CRS in 12 out of 13 trials. 35 The concentration of IFN-γ typically found in CRS patients (>10 pg/mL) is indeed much lower than that detected in chip experiments (>3,000 pg/mL). 15,35 However, a 100-fold increase in IFN-γ serum concentration was detected in patients suffering from severe CRS,8 which could also be observed in our tumoron-chip even after 4 days of culture. Yet, it is essential to emphasize that the model primarily replicates cytokine levels at the local tumor site, which may facilitate the recruitment of bystander immune cells, rather than cytokine levels in the bloodstream.

Interestingly, we noticed differences in cytokine concentrations depending on the CAR-T cell donor used for perfusion, although the fold change values typically decreased to below 20 on day 6 for both CAR-T cell donors tested (Figure S4C). This also demonstrated the applicability of this model for safety evaluations of different CAR-T cell products before administering them to patients, as cell-intrinsic effects, such as the transcriptional features of CAR-T cells, have been associated with adverse effects.³⁶ Furthermore, our data show a similar pattern of onset and kinetics for IL-2, IL-10, and TNF- α secretion, as observed in patients suffering from high-grade CRS, although on a shorter time scale.^{8,37} Further tests and extensive benchmarking with clinical data ("real-world datasets") may elucidate whether the absolute and fold change values obtained in the chip model can be graded as "toxic" or "non-toxic."

Another cytokine, IL-6, that has been identified as one of the key mediators in CRS development.³⁸ was also shown to be elevated on day 1 or 2 after CAR-T cell perfusion in our tumoron-chip models. High serum IL-6 levels are frequently detected in patients who suffer from severe CRS, and blocking IL-6 signaling (e.g., with tocilizumab) together with systemic immunosuppression via corticosteroids is the current standard of care in CRS management. 8,39-45 Although we observed an increase in IL-6 production in the CAR-T cell condition at almost all time points and for different donors, importantly, our model did not include endogenous innate immune cells such as macrophages and monocytes, which are the main sources of IL-6 that eventually induces systemic inflammation.⁴⁶ Incorporation of these cells into the model in the future will therefore be crucial for further understanding their role in the amplification and perpetuation of the proinflammatory cycle that may lead to CRS. For this reason, tocilizumab is arguably not the best option to test CRS intervention in our tumor-on-chip, and interfering directly with CAR-T cell function, e.g., with dasatinib, provides a better alternative. In this regard, such an on/off switch that modulates activation and proliferation of CAR-T cells would be a CRS mitigation strategy that acts directly on the cells that induce CRS in this setting. 47 Dasatinib temporarily inactivates CAR-T cells without negatively affecting their viability¹² and thus can be applied to manage acute toxicity.21 By applying dasatinib at different

Article



time points and for varying durations, we identified an optimal strategy to control CR while maintaining CAR-T cell efficacy throughout a 1-week period.

In the experiments that incorporated the PDOs, we refined the model by integrating isogenic hiPSC-ECs. Our cytokine secretion data showed higher fold changes in TNF- α , IFN- γ , and granzyme B levels when T cells were cocultured with mvECs from multiple donors than when T cells were cultured with isogenic hiPSC-ECs. The fold change in cytokine levels in the isogenic setting remained similar to that in the condition without ECs (Figure S3E). HiPSC-ECs were confirmed to express CD31 prior to integration into the chip (Figure S3F). Despite enabling human leukocyte antigen (HLA)-matched autologous systems, hiPSCs-ECs expressed a certain level of ROR1 (Figure S3G), which induced IFN-γ and granzyme B secretion in our plate assay (Figure S3H). Indeed, ROR1 is not only a tumor antigen but also a known marker of stem cell derivatives.⁴⁸ Despite the resulting background activation, patient-specific effects due to relative ROR1 expression by the PDOs could be detected in the tumor-on-chip models. This would not be relevant for different types of CARs, and future advances in our understanding of EC maturation should allow us to minimize this effect for ROR1-CAR-T cells.

In conclusion, our model provides the foundation for studying different roles of cell types and composition as well as biophysical barriers in altering CAR-T cell safety and efficacy for solid tumors in vitro, while it also facilitates the examination of patient-specific effects, thereby offering new opportunities for advancing both mechanistic research and clinical translation of safer CAR-T cell products.

Limitations of the study

In terms of efficacy, our model does not yet fully mimic an immunosuppressive TME with stromal cells, immunosuppressive myeloid cells, and increased extracellular matrix deposition, which are among the factors of why CAR-T cells remain ineffective for solid tumors. 49 Also, fully recapitulating mechanisms of CRS development over several days/weeks as it occurs in patients would require increasing the complexity of the current model, which is beyond the scope of the study. As already mentioned, this model does not include macrophages and monocytes, which have central involvement in initiating and perpetuating CRS. 38,46,50 Assessing additional systemic CRS biomarkers (e.g., C-reactive protein, ferritin) would require fluidic coupling with other organ-on-chip models (e.g., liver-on-chip), as certain biomarkers are produced systemically through interorgan crosstalk.51 Perfusing the (CAR-)T cells for only 20 h and subsequently removing them from the circulation from days 1-8 may also disregard the role of circulating T cells in the release of inflammatory mediators. Moreover, the clinical value of integrating PDOs in the tumor-on-chip needs to be further validated, as PDOs from only 4 patients were tested in this proof-ofconcept pilot study. Predicting the risk of CRS development as well as CAR-T cell efficacy using this model would require the testing of large number of additional patient samples.

STAR*METHODS

Detailed methods are provided in the online version of this paper and include the following:

- KEY RESOURCES TABLE
- RESOURCE AVAILABILITY
 - Lead contact
 - Materials availability
 - o Data and code availability
- EXPERIMENTAL MODEL AND SUBJECT DETAILS
- METHOD DETAILS
 - o Tumor-on-chip concept, design and fabrication
 - Tumor and fibroblast aggregates generation
 - o Patient-derived tumor organoids generation and culture
 - o Microvascular endothelial cells isolation and culture
 - O Human induced pluripotent stem cells generation from PBMCs
 - O Human induced pluripotent stem cells-derived endothelial cells generation and culture
 - o Generation and culture of ROR1- and CD19-specific CAR-T cells
 - o Aggregates/spheroids/PDOs seeding on-chip
 - o Endothelial cells seeding, chip culture, and characterization
 - o T cell perfusion and chip culture
 - o Dasatinib treatment
 - O Allogeneic / isogenic endothelial cells (CAR-)T cells coculture for cytokine assay
- QUANTIFICATION AND STATISTICAL ANALYSIS
 - o Image acquisition and analysis
 - Cytokine quantification assay
 - o Flow cytometry staining and analysis
 - Statistics and reproducibility

SUPPLEMENTAL INFORMATION

Supplemental information can be found online at https://doi.org/10.1016/j. stem.2024.04.018.

ACKNOWLEDGMENTS

We thank all the patients and healthy donors who participated in this study. We thank Eduardo Bras, Gyuntae Bae, Garvit Sharma, and Anna-Sophie Schlemmer for assistance with the chip fabrication, Stephan Bates for technical assistance with preparing CAR-T cells, Cansu E. Önder for assistance with the flow cytometry of the organoids, the LUMC human iPSC Hotel for the generation and initial characterization of hiPSC lines from PBMCs, the Flow Cytometry Core Facilities Tal and Klinik Berg at the University of Tübingen, and the imSA-

This publication is part of the imSAVAR project, which received funding from the Innovative Medicine Initiative 2 Joint Undertaking (JU) under grant agreement no. 853988. The JU receives support from the European Union's Horizon 2020 research and innovation program and EFPIA and JDRF International. We also acknowledge funding from the Wellcome Leap Human Organs, Physiology, and Engineering (HOPE) Program. T.I.M. is supported by the European Society for Blood and Marrow Transplantation (EBMT) and the European Hematology Association (EHA) Joint Fellowship Award in the Field of Cell Therapy and Immunotherapy. M.H., M.A., and L.S. were supported by the patient advocacy group Hilfe im Kampf gegen den Krebs e.V., Würzburg, Germany, and Forschung hilft - Stiftung zur Förderung der Krebsforschung an der Universität Würzburg, Germany. M.H. and M.A. were also supported by the German Research Foundation (Deutsche Forschungsgemeinschaft [DFG], SFB-TRR 338/1 2021-452881907 [Project A02]). M.H. was also supported by the Bavarian Center for Cancer Research (Bayerisches Zentrum für Krebsforschung [BZKF], Leuchtturm Immuntherapien), German Cancer Aid (Stiftung Deutsche Krebshilfe, TransOnc Project AvantCAR.de, grant no. 70114707), the BMBF SaxoCell Cluster for Future (Project UltraCART, grant no. 03ZU1111BA), and the Fraunhofer ATTRACT Program (Project CAR DUETT). L.S. receives funding from the Interdisciplinary Center for Clinical Research (IZKF), grant no. Z-2_CSP_2022-27.

AUTHOR CONTRIBUTIONS

T.I.M. performed the chip design and fabrication as well as cell culture and chip experiments with assistance from C.T., J.R., L.L., and M.C. C.T., L.L., and L.S.



performed the well-plate assays of preliminary 2D experiments. C.T. and A.K. performed the flow cytometry and analyzed the data. A.K. provided the organoids. M.A. and M.H. provided the (CAR-)T cells, tumor cell line MDA-MB-231 GFP-ffluc, PBMCs for hiPSC generation, and intellectual expertise on CAR-T cell engineering. F.E.v.d.H. and V.O. provided the hiPSCs and hiPSC-derived endothelial cells and performed their characterization. T.I.M., M.C., M.A., and P.L. designed the study. T.I.M. performed the imaging and image data analysis. T.I.M. analyzed the data from the chip experiments. T.I.M. wrote the manuscript with support from P.L., M.C., C.T., A.K., V.O., M.A., and M.H. This work was jointly supervised by P.L. and M.A., who share senior authorship. All authors have read the manuscript and provided input and agree with its submission.

DECLARATION OF INTERESTS

M.H. is an inventor on patent applications and has been granted patents related to CAR technology, licensed in part to industry. M.H. is a cofounder and equity owner of T-CURX GmbH, Würzburg. M.H. receives speaker honoraria from BMS, Janssen, Kite/Gilead, and Novartis and research support from BMS.

Received: October 5, 2023 Revised: February 22, 2024 Accepted: April 22, 2024 Published: May 15, 2024

REFERENCES

- Utkarsh, K., Srivastava, N., Kumar, S., Khan, A., Dagar, G., Kumar, M., Singh, M., and Haque, S. (2024). CAR-T cell therapy: a game-changer in cancer treatment and beyond. Clin. Transl. Oncol. https://doi.org/10. 1007/s12094-023-03368-2.
- Scheller, L., Tebuka, E., Rambau, P.F., Einsele, H., Hudecek, M., Prommersberger, S.R., and Danhof, S. (2024). BCMA CAR-T cells in multiple myeloma-ready for take-off? Leuk. Lymphoma 65, 143–157. https://doi.org/10.1080/10428194.2023.2276676.
- Chen, N., Li, X., Chintala, N.K., Tano, Z.E., and Adusumilli, P.S. (2018).
 Driving CARs on the uneven road of antigen heterogeneity in solid tumors.
 Curr. Opin. Immunol. 51, 103–110. https://doi.org/10.1016/j.coi.2018.
 03.002.
- Kankeu Fonkoua, L.A., Sirpilla, O., Sakemura, R., Siegler, E.L., and Kenderian, S.S. (2022). CAR T cell therapy and the tumor microenvironment: Current challenges and opportunities. Mol. Ther. Oncolytics 25, 69–77. https://doi.org/10.1016/j.omto.2022.03.009.
- Duncan, B.B., Dunbar, C.E., and Ishii, K. (2022). Applying a clinical lens to animal models of CAR-T cell therapies. Mol. Ther. Methods Clin. Dev. 27, 17–31. https://doi.org/10.1016/j.cmtm.2022.08.008.
- Albelda, S.M. (2024). CAR T cell therapy for patients with solid tumours: key lessons to learn and unlearn. Nat. Rev. Clin. Oncol. 21, 47–66. https://doi.org/10.1038/s41571-023-00832-4.
- Choi, Y., Lee, S., Kim, K., Kim, S.-H., Chung, Y.-J., and Lee, C. (2018). Studying cancer immunotherapy using patient-derived xenografts (PDXs) in humanized mice. Exp. Mol. Med. 50, 1–12. https://doi.org/10. 1038/s12276-018-0115-0.
- Morris, E.C., Neelapu, S.S., Giavridis, T., and Sadelain, M. (2022). Cytokine release syndrome and associated neurotoxicity in cancer immunotherapy. Nat. Rev. Immunol. 22, 85–96. https://doi.org/10.1038/s41577-021-00547-6.
- Maulana, T.I., Kromidas, E., Wallstabe, L., Cipriano, M., Alb, M., Zaupa, C., Hudecek, M., Fogal, B., and Loskill, P. (2021). Immunocompetent canceron-chip models to assess immuno-oncology therapy. Adv. Drug Deliv. Rev. 173, 281–305. https://doi.org/10.1016/j.addr.2021.03.015.
- Cipriano, M., Schlünder, K., Probst, C., Linke, K., Weiss, M., Fischer, M.J., Mesch, L., Achberger, K., Liebau, S., Mesquida, M., et al. (2022). Human immunocompetent choroid-on-chip: a novel tool for studying ocular ef-

- fects of biological drugs. Commun. Biol. 5, 52. https://doi.org/10.1038/s42003-021-02977-3
- Rogal, J., Roosz, J., Teufel, C., Cipriano, M., Xu, R., Eisler, W., Weiss, M., Schenke-Layland, K., and Loskill, P. (2022). Autologous Human Immunocompetent White Adipose Tissue-on-Chip. Adv. Sci. (Weinh) 9, e2104451. https://doi.org/10.1002/advs.202104451.
- Mestermann, K., Giavridis, T., Weber, J., Rydzek, J., Frenz, S., Nerreter, T., Mades, A., Sadelain, M., Einsele, H., and Hudecek, M. (2019). The tyrosine kinase inhibitor dasatinib acts as a pharmacologic on/off switch for CAR T cells. Sci. Transl. Med. 11, eaau5907. https://doi.org/10.1126/sci-translmed.aau5907.
- Önder, C.E., Ziegler, T.J., Becker, R., Brucker, S.Y., Hartkopf, A.D., Engler, T., and Koch, A. (2023). Advancing Cancer Therapy Predictions with Patient-Derived Organoid Models of Metastatic Breast Cancer. Cancers 15, 3602. https://doi.org/10.3390/cancers15143602.
- Turtle, C.J., Hanafi, L.A., Berger, C., Hudecek, M., Pender, B., Robinson, E., Hawkins, R., Chaney, C., Cherian, S., Chen, X., et al. (2016).
 Immunotherapy of non-Hodgkin's lymphoma with a defined ratio of CD8+ and CD4+ CD19-specific chimeric antigen receptor-modified T cells. Sci. Transl. Med. 8, 355ra116. https://doi.org/10.1126/scitranslmed.aaf8621
- Turtle, C.J., Hanafi, L.A., Berger, C., Gooley, T.A., Cherian, S., Hudecek, M., Sommermeyer, D., Melville, K., Pender, B., Budiarto, T.M., et al. (2016). CD19 CAR-T cells of defined CD4+:CD8+ composition in adult B cell ALL patients. J. Clin. Invest. 126, 2123–2138. https://doi.org/10. 1172/JCI85309.
- Lee, D.W., Santomasso, B.D., Locke, F.L., Ghobadi, A., Turtle, C.J., Brudno, J.N., Maus, M.V., Park, J.H., Mead, E., Pavletic, S., et al. (2019). ASTCT Consensus Grading for Cytokine Release Syndrome and Neurologic Toxicity Associated with Immune Effector Cells. Biol. Blood Marrow Transplant. 25, 625–638. https://doi.org/10.1016/j.bbmt.2018. 12.758.
- Clerbaux, L.-A., Filipovska, J., Nymark, P., Chauhan, V., Sewald, K., Alb, M., Sachana, M., Beronius, A., Amorim, M.-J., and Wittwehr, C. (2024). Beyond chemicals: Opportunities and challenges of integrating non-chemical stressors in adverse outcome pathways. ALTEX 41, 233–247. https://doi.org/10.14573/altex.2307061.
- Alb, M., Reiche, K., Rade, M., Sewald, K., Loskill, P., Cipriano, M., Maulana, T.I., van der Meer, A., Weener, H., Patel, N., et al. (2024). Novel strategies to assess cytokine release mediated by chimeric antigen receptor T cells based on the adverse outcome pathway concept. J. Immunotoxicol. https://doi.org/10.1080/1547691X.2024.2345158.
- Donnadieu, E., Luu, M., Alb, M., Anliker, B., Arcangeli, S., Bonini, C., De Angelis, B., Choudhary, R., Espie, D., Galy, A., et al. (2022). Time to evolve: predicting engineered T cell-associated toxicity with next-generation models. J. Immunother. Cancer 10, e003486. https://doi.org/10.1136/ iitr-2021-003486
- Rafiq, S., Hackett, C.S., and Brentjens, R.J. (2020). Engineering strategies to overcome the current roadblocks in CAR T cell therapy. Nat. Rev. Clin. Oncol. 17, 147–167. https://doi.org/10.1038/s41571-019-0297-y.
- Baur, K., Heim, D., Beerlage, A., Poerings, A.S., Kopp, B., Medinger, M., Dirks, J.C., Passweg, J.R., and Holbro, A. (2022). Dasatinib for treatment of CAR T-cell therapy-related complications. J. Immunother. Cancer 10, e005956. https://doi.org/10.1136/jitc-2022-005956.
- Zhang, S., Chen, L., Wang-Rodriguez, J., Zhang, L., Cui, B., Frankel, W., Wu, R., and Kipps, T.J. (2012). The Onco-Embryonic Antigen ROR1 Is Expressed by a Variety of Human Cancers. Am. J. Pathol. 181, 1903– 1910. https://doi.org/10.1016/j.ajpath.2012.08.024.
- Balakrishnan, A., Goodpaster, T., Randolph-Habecker, J., Hoffstrom, B.G., Jalikis, F.G., Koch, L.K., Berger, C., Kosasih, P.L., Rajan, A., Sommermeyer, D., et al. (2017). Analysis of ROR1 Protein Expression in Human Cancer and Normal Tissues. Clin. Cancer Res. 23, 3061–3071. https://doi.org/10.1158/1078-0432.CCR-16-2083.

Article



- Joyce, J.A., and Fearon, D.T. (2015). T cell exclusion, immune privilege, and the tumor microenvironment. Science 348, 74–80. https://doi.org/ 10.1126/science.aaa6204.
- Jiang, P., Gu, S., Pan, D., Fu, J., Sahu, A., Hu, X., Li, Z., Traugh, N., Bu, X., Li, B., et al. (2018). Signatures of T cell dysfunction and exclusion predict cancer immunotherapy response. Nat. Med. 24, 1550–1558. https://doi. org/10.1038/s41591-018-0136-1.
- Lanitis, E., Irving, M., and Coukos, G. (2015). Targeting the tumor vasculature to enhance T cell activity. Curr. Opin. Immunol. 33, 55–63. https://doi.org/10.1016/j.coi.2015.01.011.
- Huang, Y., Kim, B.Y.S., Chan, C.K., Hahn, S.M., Weissman, I.L., and Jiang, W. (2018). Improving immune–vascular crosstalk for cancer immunotherapy. Nat. Rev. Immunol. 18, 195–203. https://doi.org/10.1038/nri. 2017.145.
- Dekkers, J.F., Alieva, M., Cleven, A., Keramati, F., Wezenaar, A.K.L., van Vliet, E.J., Puschhof, J., Brazda, P., Johanna, I., Meringa, A.D., et al. (2023). Uncovering the mode of action of engineered T cells in patient cancer organoids. Nat. Biotechnol. 41, 60–69. https://doi.org/10.1038/s41587-022-01397-w.
- Yu, L., Li, Z., Mei, H., Li, W., Chen, D., Liu, L., Zhang, Z., Sun, Y., Song, F., Chen, W., et al. (2021). Patient-derived organoids of bladder cancer recapitulate antigen expression profiles and serve as a personal evaluation model for CAR-T cells *in vitro*. Clin. Transl. Immunology *10*, e1248. https://doi.org/10.1002/cti2.1248.
- Jacob, F., Ming, G.L., and Song, H. (2020). Generation and biobanking of patient-derived glioblastoma organoids and their application in CART cell testing. Nat. Protoc. 15, 4000–4033. https://doi.org/10.1038/s41596-020-0402-9.
- Arenas, E.J., Martínez-Sabadell, A., Rius Ruiz, I., Román Alonso, M., Escorihuela, M., Luque, A., Fajardo, C.A., Gros, A., Klein, C., and Arribas, J. (2021). Acquired cancer cell resistance to T cell bispecific antibodies and CAR T targeting HER2 through JAK2 down-modulation. Nat. Commun. 12, 1237. https://doi.org/10.1038/s41467-021-21445-4.
- Schnalzger, T.E., de Groot, M.H., Zhang, C., Mosa, M.H., Michels, B.E., Röder, J., Darvishi, T., Wels, W.S., and Farin, H.F. (2019). 3D model for CAR-mediated cytotoxicity using patient-derived colorectal cancer organoids. EMBO J. 38, e100928. https://doi.org/10.15252/embj.2018100928.
- Önder, C.E., Moustafa-Oglou, M., Schröder, S.M., Hartkopf, A.D., Koch, A., and Seitz, C.M. (2023). Precision Immunotherapy Utilizing Adapter CAR-T Cells (AdCAR-T) in Metastatic Breast Cancer Leads to Target Specific Lysis. Cancers 16, 168. https://doi.org/10.3390/cancers16010168.
- Teachey, D.T., Lacey, S.F., Shaw, P.A., Melenhorst, J.J., Maude, S.L., Frey, N., Pequignot, E., Gonzalez, V.E., Chen, F., Finklestein, J., et al. (2016). Identification of Predictive Biomarkers for Cytokine Release Syndrome after Chimeric Antigen Receptor T-cell Therapy for Acute Lymphoblastic Leukemia. Cancer Discov. 6, 664–679. https://doi.org/10. 1158/2159-8290.CD-16-0040.
- Tedesco, V.E., and Mohan, C. (2021). Biomarkers for Predicting Cytokine Release Syndrome following CD19-Targeted CAR T Cell Therapy.
 J. Immunol. 206, 1561–1568. https://doi.org/10.4049/jimmunol.2001249.
- Deng, Q., Han, G., Puebla-Osorio, N., Ma, M.C.J., Strati, P., Chasen, B., Dai, E., Dang, M., Jain, N., Yang, H., et al. (2020). Characteristics of anti-CD19 CAR T cell infusion products associated with efficacy and toxicity in patients with large B cell lymphomas. Nat. Med. 26, 1878–1887. https://doi.org/10.1038/s41591-020-1061-7.
- Hay, K.A., Hanafi, L.A., Li, D., Gust, J., Liles, W.C., Wurfel, M.M., López, J.A., Chen, J., Chung, D., Harju-Baker, S., et al. (2017). Kinetics and biomarkers of severe cytokine release syndrome after CD19 chimeric antigen receptor-modified T-cell therapy. Blood 130, 2295–2306. https://doi.org/ 10.1182/blood-2017-06-793141.
- Norelli, M., Camisa, B., Barbiera, G., Falcone, L., Purevdorj, A., Genua, M., Sanvito, F., Ponzoni, M., Doglioni, C., Cristofori, P., et al. (2018). Monocyte-derived IL-1 and IL-6 are differentially required for cytokine-release syndrome and neurotoxicity due to CAR T cells. Nat. Med. 24, 739–748. https://doi.org/10.1038/s41591-018-0036-4.

- Maude, S.L., Frey, N., Shaw, P.A., Aplenc, R., Barrett, D.M., Bunin, N.J., Chew, A., Gonzalez, V.E., Zheng, Z., Lacey, S.F., et al. (2014). Chimeric Antigen Receptor T Cells for Sustained Remissions in Leukemia. N. Engl. J. Med. 371, 1507–1517. https://doi.org/10.1056/NEJMoa1407222.
- Lee, D.W., Kochenderfer, J.N., Stetler-Stevenson, M., Cui, Y.K., Delbrook, C., Feldman, S.A., Fry, T.J., Orentas, R., Sabatino, M., Shah, N.N., et al. (2015). T cells expressing CD19 chimeric antigen receptors for acute lymphoblastic leukaemia in children and young adults: a phase 1 doseescalation trial. Lancet 385, 517–528. https://doi.org/10.1016/S0140-6736(14)61403-3.
- Grupp, S.A., Kalos, M., Barrett, D., Aplenc, R., Porter, D.L., Rheingold, S.R., Teachey, D.T., Chew, A., Hauck, B., Wright, J.F., et al. (2013). Chimeric antigen receptor-modified T cells for acute lymphoid leukemia. N. Engl. J. Med. 368, 1509–1518. https://doi.org/10.1056/NEJMoa1215134.
- Neelapu, S.S., Tummala, S., Kebriaei, P., Wierda, W., Gutierrez, C., Locke, F.L., Komanduri, K.V., Lin, Y., Jain, N., Daver, N., et al. (2018). Chimeric antigen receptor T-cell therapy — assessment and management of toxicities. Nat. Rev. Clin. Oncol. 15, 47–62. https://doi.org/10.1038/nrclinonc. 2017 148
- Neelapu, S.S. (2019). Managing the toxicities of CAR T-cell therapy. Hematol. Oncol. 37 (Suppl 1), 48–52. https://doi.org/10.1002/hon.2595.
- Neelapu, S.S., Locke, F.L., Bartlett, N.L., Lekakis, L.J., Miklos, D.B., Jacobson, C.A., Braunschweig, I., Oluwole, O.O., Siddiqi, T., Lin, Y., et al. (2017). Axicabtagene Ciloleucel CAR T-Cell Therapy in Refractory Large B-Cell Lymphoma. N. Engl. J. Med. 377, 2531–2544. https://doi. org/10.1056/NEJMoa1707447.
- Maude, S.L., Laetsch, T.W., Buechner, J., Rives, S., Boyer, M., Bittencourt, H., Bader, P., Verneris, M.R., Stefanski, H.E., Myers, G.D., et al. (2018). Tisagenlecleucel in Children and Young Adults with B-Cell Lymphoblastic Leukemia. N. Engl. J. Med. 378, 439–448. https://doi. org/10.1056/NEJMoa1709866.
- Giavridis, T., van der Stegen, S.J.C., Eyquem, J., Hamieh, M., Piersigilli, A., and Sadelain, M. (2018). CAR T cell-induced cytokine release syndrome is mediated by macrophages and abated by IL-1 blockade. Nat. Med. 24, 731–738. https://doi.org/10.1038/s41591-018-0041-7.
- 47. Xiao, X., Huang, S., Chen, S., Wang, Y., Sun, Q., Xu, X., and Li, Y. (2021). Mechanisms of cytokine release syndrome and neurotoxicity of CAR T-cell therapy and associated prevention and management strategies. J. Exp. Clin. Cancer Res. 40, 367. https://doi.org/10.1186/s13046-021-02148-6.
- Halloin, C., Schwanke, K., Löbel, W., Franke, A., Szepes, M., Biswanath, S., Wunderlich, S., Merkert, S., Weber, N., Osten, F., et al. (2019). Continuous WNT Control Enables Advanced hPSC Cardiac Processing and Prognostic Surface Marker Identification in Chemically Defined Suspension Culture. Stem Cell Rep. 13, 366–379. https://doi.org/10. 1016/j.stemcr.2019.06.004.
- Hou, A.J., Chen, L.C., and Chen, Y.Y. (2021). Navigating CAR-T cells through the solid-tumour microenvironment. Nat. Rev. Drug Discov. 20, 531–550. https://doi.org/10.1038/s41573-021-00189-2.
- Liu, Y., Fang, Y., Chen, X., Wang, Z., Liang, X., Zhang, T., Liu, M., Zhou, N., Lv, J., Tang, K., et al. (2020). Gasdermin E-mediated target cell pyroptosis by CAR T cells triggers cytokine release syndrome. Sci. Immunol. 5, eaax7969. https://doi.org/10.1126/sciimmunol.aax7969.
- Shimabukuro-Vornhagen, A., Gödel, P., Subklewe, M., Stemmler, H.J., Schlößer, H.A., Schlaak, M., Kochanek, M., Böll, B., and Von Bergwelt-Baildon, M.S. (2018). Cytokine release syndrome. J. Immunother. Cancer 6, 56. https://doi.org/10.1186/s40425-018-0343-9.
- Schindelin, J., Arganda-Carreras, I., Frise, E., Kaynig, V., Longair, M., Pietzsch, T., Preibisch, S., Rueden, C., Saalfeld, S., Schmid, B., et al. (2012). Fiji: an open-source platform for biological-image analysis. Nat. Methods 9, 676–682. https://doi.org/10.1038/nmeth.2019.
- Okita, K., Matsumura, Y., Sato, Y., Okada, A., Morizane, A., Okamoto, S., Hong, H., Nakagawa, M., Tanabe, K., Tezuka, K., et al. (2011). A more efficient method to generate integration-free human iPS cells. Nat. Methods 8, 409–412. https://doi.org/10.1038/nmeth.1591.



- Rogal, J., Binder, C., Kromidas, E., Roosz, J., Probst, C., Schneider, S., Schenke-Layland, K., and Loskill, P. (2020). WAT-on-a-chip integrating human mature white adipocytes for mechanistic research and pharmaceutical applications. Sci. Rep. 10, 6666. https://doi.org/10.1038/s41598-020-63710-4.
- Xia, Y., and Whitesides, G.M. (1998). Soft lithography. Annu. Rev. Mater. Sci. 28, 153–184. https://doi.org/10.1146/annurev.matsci.28.1.153.
- Dahlmann, J., Kensah, G., Kempf, H., Skvorc, D., Gawol, A., Elliott, D.A., Dräger, G., Zweigerdt, R., Martin, U., and Gruh, I. (2013). The use of agarose microwells for scalable embryoid body formation and cardiac differentiation of human and murine pluripotent stem cells. Biomaterials 34, 2463–2471. https://doi.org/10.1016/j.biomaterials.2012.12.024.
- Miyoshi, H., and Stappenbeck, T.S. (2013). In vitro expansion and genetic modification of gastrointestinal stem cells in spheroid culture. Nat. Protoc. 8, 2471–2482. https://doi.org/10.1038/nprot.2013.153.
- Bouma, M.J., Van Iterson, M., Janssen, B., Mummery, C.L., Salvatori, D.C.F., and Freund, C. (2017). Differentiation-Defective Human Induced Pluripotent Stem Cells Reveal Strengths and Limitations of the Teratoma Assay and In Vitro Pluripotency Assays. Stem Cell Rep. 8, 1340–1353. https://doi.org/10.1016/j.stemcr.2017.03.009.
- Dambrot, C., Van De Pas, S., Van Zijl, L., Brändl, B., Wang, J.W., Schalij, M.J., Hoeben, R.C., Atsma, D.E., Mikkers, H.M., Mummery, C.L., and Freund, C. (2013). Polycistronic lentivirus induced pluripotent stem cells from skin biopsies after long term storage, blood outgrowth endothelial cells and cells from milk teeth. Differentiation 85, 101–109. https://doi. org/10.1016/j.diff.2013.01.001.
- Freund, C., Davis, R.P., Gkatzis, K., Ward-van Oostwaard, D., and Mummery, C.L. (2010). The first reported generation of human induced

- pluripotent stem cells (iPS cells) and iPS cell-derived cardiomyocytes in the Netherlands. Neth. Heart J. 18, 51–54.
- 61. Westen, A.A., Kraaijenbrink, T., Robles De Medina, E.A., Harteveld, J., Willemse, P., Zuniga, S.B., Van Der Gaag, K.J., Weiler, N.E.C., Warnaar, J., Kayser, M., et al. (2014). Comparing six commercial autosomal STR kits in a large Dutch population sample. Forensic Sci. Int. Genet. 10, 55–63. https://doi.org/10.1016/j.fsigen.2014.01.008.
- Orlova, V.V., van den Hil, F.E., Petrus-Reurer, S., Drabsch, Y., ten Dijke, P., and Mummery, C.L. (2014). Generation, expansion and functional analysis of endothelial cells and pericytes derived from human pluripotent stem cells. Nat. Protoc. 9, 1514–1531. https://doi.org/10.1038/nprot.2014.102.
- Hudecek, M., Lupo-Stanghellini, M.-T., Kosasih, P.L., Sommermeyer, D., Jensen, M.C., Rader, C., and Riddell, S.R. (2013). Receptor affinity and extracellular domain modifications affect tumor recognition by ROR1-specific chimeric antigen receptor T cells. Clin. Cancer Res. 19, 3153–3164. https://doi.org/10.1158/1078-0432.CCR-13-0330.
- Sommermeyer, D., Hudecek, M., Kosasih, P.L., Gogishvili, T., Maloney, D.G., Turtle, C.J., and Riddell, S.R. (2016). Chimeric antigen receptormodified T cells derived from defined CD8+ and CD4+ subsets confer superior antitumor reactivity in vivo. Leukemia 30, 492–500. https://doi.org/ 10.1038/leu.2015.247.
- Ostroumov, D., Fekete-Drimusz, N., Saborowski, M., Kühnel, F., and Woller, N. (2018). CD4 and CD8 T lymphocyte interplay in controlling tumor growth. Cell. Mol. Life Sci. 75, 689–713. https://doi.org/10.1007/s00018-017-2686-7.
- Raskov, H., Orhan, A., Christensen, J.P., and Gögenur, I. (2021). Cytotoxic CD8+ T cells in cancer and cancer immunotherapy. Br. J. Cancer 124, 359–367. https://doi.org/10.1038/s41416-020-01048-4.

Article



STAR***METHODS**

KEY RESOURCES TABLE

REAGENT or RESOURCE	SOURCE	IDENTIFIER
Antibodies	OOOHOL	IDENTIFIER
ROR1 Antibody, anti-human, REAfinity	Miltenyi Biotec	130-118-015; RRID: AB_2733448
(fin.conc. 1:100)	Willierly Diotec	130-110-013, 11111 <i>D</i> . Ab_2100440
CD31 Antibody, anti-human, REAfinity (fin.conc.1:50)	Miltenyi Biotec	130-110-808; RRID: AB_2657282
PE/Cyanine7 anti-human CD3 Antibody (fin.conc. 1:400)	BioLegend	317334; RRID: AB_2561452
APC/Fire 750 anti-human CD4 Antibody (fin.conc. 1:100)	BioLegend	357426; RRID: AB_2716183
PerCP anti-human CD8a Antibody (fin.conc. 1:50)	BioLegend	300922; RRID: AB_1575072
Brilliant Violet 421 anti-human CD25 Antibody (fin.conc. 1:50)	BioLegend	302630; RRID: AB_11126749
FITC anti-human CD69 Antibody (fin.conc.1:50)	BioLegend	310904; RRID: AB_314839
CD31 Antibody, anti-human (fin. conc. 1:50)	DAKO	M0823; RRID: AB_2114471
VE-cadherin Antibody, anti-human (fin. conc. 1:50)	Invitrogen	36-1900; RRID: AB_2533243
Goat anti-Mouse IgG (H+L), Superclonal Recombinant Secondary Antibody, AlexaFluor 647 (fin. conc. 1:100)	Invitrogen	A28181; RRID: AB_2536165
Goat anti-Rabbit IgG (Heavy chain), Superclonal Recombinant Secondary Antibody, Alexa Fluor 555 (f.c. 1:100)	Invitrogen	A27039; RRID: AB_2536100
Biological samples		
Primary tumor materials to generate PDOs	Women's Hospital, University of Tübingen,	Table S1
	Germany	
Resected skin tissue to isolate mvECs	Germany Klinik Charlottenhaus, Stuttgart, Germany	See experimental model and subject details
PBMCs to generate CAR-T cells and	•	
PBMCs to generate CAR-T cells and niPSCs	Klinik Charlottenhaus, Stuttgart, Germany	See experimental model and subject details
PBMCs to generate CAR-T cells and niPSCs Chemicals, peptides, and recombinant proteins	Klinik Charlottenhaus, Stuttgart, Germany	
PBMCs to generate CAR-T cells and niPSCs Chemicals, peptides, and recombinant proteins SYLGARD 184 silicone elastomer	Klinik Charlottenhaus, Stuttgart, Germany DRK Frankfurt, Germany	See experimental model and subject detail
PBMCs to generate CAR-T cells and niPSCs Chemicals, peptides, and recombinant proteins SYLGARD 184 silicone elastomer Hydrosil 1:1 Cultrex Reduced Growth Factor Basement	Klinik Charlottenhaus, Stuttgart, Germany DRK Frankfurt, Germany Dow Corning	See experimental model and subject detail 5498840000
PBMCs to generate CAR-T cells and hiPSCs Chemicals, peptides, and recombinant proteins SYLGARD 184 silicone elastomer Hydrosil 1:1 Cultrex Reduced Growth Factor Basement Membrane Extract, Type 2 Select	Klinik Charlottenhaus, Stuttgart, Germany DRK Frankfurt, Germany Dow Corning SILADENT	See experimental model and subject detail 5498840000 101301
PBMCs to generate CAR-T cells and niPSCs Chemicals, peptides, and recombinant proteins SYLGARD 184 silicone elastomer Hydrosil 1:1 Cultrex Reduced Growth Factor Basement Membrane Extract, Type 2 Select TrypLE Express	Klinik Charlottenhaus, Stuttgart, Germany DRK Frankfurt, Germany Dow Corning SILADENT Bio-Techne	See experimental model and subject detail 5498840000 101301 3533-005-02
PBMCs to generate CAR-T cells and hiPSCs Chemicals, peptides, and recombinant proteins SYLGARD 184 silicone elastomer Hydrosil 1:1 Cultrex Reduced Growth Factor Basement Membrane Extract, Type 2 Select TrypLE Express TrypLE Select	Klinik Charlottenhaus, Stuttgart, Germany DRK Frankfurt, Germany Dow Corning SILADENT Bio-Techne Gibco	See experimental model and subject detail 5498840000 101301 3533-005-02 12604013
PBMCs to generate CAR-T cells and hiPSCs Chemicals, peptides, and recombinant proteins SYLGARD 184 silicone elastomer Hydrosil 1:1 Cultrex Reduced Growth Factor Basement Membrane Extract, Type 2 Select TrypLE Express TrypLE Select GlutaMAX	Klinik Charlottenhaus, Stuttgart, Germany DRK Frankfurt, Germany Dow Corning SILADENT Bio-Techne Gibco Gibco	See experimental model and subject detail 5498840000 101301 3533-005-02 12604013 12563-029
PBMCs to generate CAR-T cells and hiPSCs Chemicals, peptides, and recombinant proteins SYLGARD 184 silicone elastomer Hydrosil 1:1 Cultrex Reduced Growth Factor Basement Membrane Extract, Type 2 Select TrypLE Express TrypLE Select GlutaMAX HEPES	Klinik Charlottenhaus, Stuttgart, Germany DRK Frankfurt, Germany Dow Corning SILADENT Bio-Techne Gibco Gibco Thermo Fisher	See experimental model and subject detail 5498840000 101301 3533-005-02 12604013 12563-029 35050-038
PBMCs to generate CAR-T cells and hiPSCs Chemicals, peptides, and recombinant proteins SYLGARD 184 silicone elastomer Hydrosil 1:1 Cultrex Reduced Growth Factor Basement Membrane Extract, Type 2 Select TrypLE Express TrypLE Select GlutaMAX HEPES Gentamicin	Klinik Charlottenhaus, Stuttgart, Germany DRK Frankfurt, Germany Dow Corning SILADENT Bio-Techne Gibco Gibco Thermo Fisher Thermo Fisher	See experimental model and subject detail 5498840000 101301 3533-005-02 12604013 12563-029 35050-038 15630-056
PBMCs to generate CAR-T cells and hiPSCs Chemicals, peptides, and recombinant proteins SYLGARD 184 silicone elastomer Hydrosil 1:1 Cultrex Reduced Growth Factor Basement Membrane Extract, Type 2 Select TrypLE Express TrypLE Select GlutaMAX HEPES Gentamicin Hoechst 33342	Klinik Charlottenhaus, Stuttgart, Germany DRK Frankfurt, Germany Dow Corning SILADENT Bio-Techne Gibco Gibco Thermo Fisher Thermo Fisher Thermo Fisher	See experimental model and subject detail 5498840000 101301 3533-005-02 12604013 12563-029 35050-038 15630-056 15710049
PBMCs to generate CAR-T cells and hiPSCs Chemicals, peptides, and recombinant proteins SYLGARD 184 silicone elastomer Hydrosil 1:1 Cultrex Reduced Growth Factor Basement Membrane Extract, Type 2 Select TrypLE Express TrypLE Select GlutaMAX HEPES Gentamicin Hoechst 33342 327 Supplement	Klinik Charlottenhaus, Stuttgart, Germany DRK Frankfurt, Germany Dow Corning SILADENT Bio-Techne Gibco Gibco Thermo Fisher Thermo Fisher Thermo Fisher Thermo Fisher	See experimental model and subject detail 5498840000 101301 3533-005-02 12604013 12563-029 35050-038 15630-056 15710049 62249
PBMCs to generate CAR-T cells and niPSCs Chemicals, peptides, and recombinant proteins SYLGARD 184 silicone elastomer Hydrosil 1:1 Cultrex Reduced Growth Factor Basement Membrane Extract, Type 2 Select TrypLE Express TrypLE Select GlutaMAX HEPES Gentamicin Hoechst 33342 B27 Supplement Heregulinß-1	Klinik Charlottenhaus, Stuttgart, Germany DRK Frankfurt, Germany Dow Corning SILADENT Bio-Techne Gibco Gibco Thermo Fisher Thermo Fisher Thermo Fisher Thermo Fisher Thermo Fisher Thermo Fisher	See experimental model and subject detail 5498840000 101301 3533-005-02 12604013 12563-029 35050-038 15630-056 15710049 62249 17504-044
PBMCs to generate CAR-T cells and hiPSCs Chemicals, peptides, and recombinant proteins SYLGARD 184 silicone elastomer Hydrosil 1:1 Cultrex Reduced Growth Factor Basement Membrane Extract, Type 2 Select TrypLE Express TrypLE Select GlutaMAX HEPES Gentamicin Hoechst 33342 B27 Supplement Heregulinß-1 FGF7	Klinik Charlottenhaus, Stuttgart, Germany DRK Frankfurt, Germany Dow Corning SILADENT Bio-Techne Gibco Gibco Thermo Fisher Thermo Fisher Thermo Fisher Thermo Fisher Thermo Fisher PeproTech	See experimental model and subject detail 5498840000 101301 3533-005-02 12604013 12563-029 35050-038 15630-056 15710049 62249 17504-044 100-03
Resected skin tissue to isolate mvECs PBMCs to generate CAR-T cells and hiPSCs Chemicals, peptides, and recombinant proteins SYLGARD 184 silicone elastomer Hydrosil 1:1 Cultrex Reduced Growth Factor Basement Membrane Extract, Type 2 Select TrypLE Express TrypLE Select GlutaMAX HEPES Gentamicin Hoechst 33342 B27 Supplement Heregulinß-1 FGF7 FGF10 EGF	Klinik Charlottenhaus, Stuttgart, Germany DRK Frankfurt, Germany Dow Corning SILADENT Bio-Techne Gibco Gibco Thermo Fisher Thermo Fisher Thermo Fisher Thermo Fisher Thermo Fisher Thermo Fisher PeproTech PeproTech	See experimental model and subject detail 5498840000 101301 3533-005-02 12604013 12563-029 35050-038 15630-056 15710049 62249 17504-044 100-03 100-19
PBMCs to generate CAR-T cells and hiPSCs Chemicals, peptides, and recombinant proteins SYLGARD 184 silicone elastomer Hydrosil 1:1 Cultrex Reduced Growth Factor Basement Membrane Extract, Type 2 Select TrypLE Express TrypLE Select GlutaMAX HEPES Gentamicin Hoechst 33342 B27 Supplement Heregulinß-1 FGF7 FGF10	Klinik Charlottenhaus, Stuttgart, Germany DRK Frankfurt, Germany Dow Corning SILADENT Bio-Techne Gibco Gibco Thermo Fisher Thermo Fisher Thermo Fisher Thermo Fisher Thermo Fisher PeproTech PeproTech PeproTech	See experimental model and subject detail 5498840000 101301 3533-005-02 12604013 12563-029 35050-038 15630-056 15710049 62249 17504-044 100-03 100-19 100-26

(Continued on next page)



Continued		
REAGENT or RESOURCE	SOURCE	IDENTIFIER
SB-202190	Sigma Aldrich	S7067
N-acetyl-cysteine	Sigma Aldrich	A9165
Nicotinamide	Sigma Aldrich	N0636
Human serum from platelet poor plasma	Sigma Aldrich	P2918
Fibronectin	Sigma Aldrich	F1141
Propidium iodide	Sigma Aldrich	P4170
DAPI	Sigma Aldrich	D8417
bFGF	Miltenyi Biotech	130-093-564
VEGF	Miltenyi Biotech	130-109-396
Dispase	Merck KGaA	D4693
EDTA	Invitrogen	15575020
CellTracker CMFDA	Invitrogen	C7025
CellTracker Deep Red	Invitrogen	C34565
3-D Life Dextran-CD Hydrogel SG	Cellendes GmbH	G93-1
FibriCol	Advanced Biomatrix	5133
Dasatinib	Selleckchem	S1021
Zombie aqua dye	BioLegend	423102
BD Fc Block	BD Biosciences	564220
ROTIHistofix 4%	Carl Roth GmbH	P087.6
Critical commercial assays		
Legendplex Human CD8/NK Mix and Match Subpanel	BioLegend	741187
Experimental models: Cell lines		
MDA-MB-231	ATCC	HTB-26
Software and algorithms		
lmageJ-Fiji	https://imagej.nih.gov/ij/	Schindelin et al. ⁵²
Imaris 9.5	https://imaris.oxinst.com/versions/9-5	N/A

RESOURCE AVAILABILITY

Lead contact

Further information and requests for resources and reagents should be directed to and will be fulfilled by the lead contact, Peter Loskill (peter.loskill@uni-tuebingen.de).

Materials availability

This study did not generate new unique reagents.

Data and code availability

- The data reported in this paper will be shared by the lead contact upon request.
- This paper does not report original code.
- Any additional information required to reanalyze the data reported in this paper is available from the lead contact upon request.

EXPERIMENTAL MODEL AND SUBJECT DETAILS

MDA-MB-231 cells were purchased from ATCC and were lentivirally transduced to express GFP-firefly luciferase fusion protein. The cells were cultured in RPMI-1640 (11835030, Thermo Fisher Scientific) supplemented with 10% (v/v) FCS (SH30066.03, HyClone FetalClone II Serum; Cytiva), 1X GlutaMAX (35050061; Thermo Fisher Scientific), and 100 U/mL penicillin-streptomycin (15140122; Thermo Fisher Scientific). Primary human fibroblasts were cultured in DMEM (41965039; Gibco) supplemented with 10% (v/v) FCS and 100 U/mL penicillin-streptomycin.

Patient-derived organoids (PDOs) were established from specimens obtained from four advanced breast cancer female patients (age 52-63) treated at the Department of Women's Health in Tübingen (detailed information is provided in Table S1). All patients gave



informed consent and the study was approved by the Ethical Committee of the Eberhard Karls University Tübingen (No. 150/2018BO2 and 662/2022BO2).

Human microvascular endothelial cells (mvECs) were isolated from resected skin tissue from plastic surgeries received from Dr. Ulrich E. Ziegler (Klinik Charlottenhaus, Stuttgart, Germany) as described previously, ¹¹ and derived from 5 donors (4 females in the age of 30, 34, 67 and unknown, and one 50 years old male). The study was approved by the local medical ethics committee: Patients gave an informed consent according to the permission of the "Landesärztekammer Baden-Württemberg" (IRB#: F-2020-166; for normal skin from elective surgeries). Sex- and gender-based analysis were not considered in the study design due to the logistical complexity of the 3 cell types cultured simultaneously, hence the experiments were conducted based on donors availability.

(CAR-)T cells were generated from two healthy female donor PBMCs obtained via apheresis procedure at the DRK Frankfurt, Germany, following informed consent for research purposes. HiPSCs were also generated from these PBMCs using episomal vectors without TP53 shRNA⁵³ according to standard protocols at the Leiden University Medical Center (LUMC) iPSC core facility.

All cells cultures were maintained in a humidified incubator at 37 °C, 5% CO₂ and 95% rH. Cell lines were routinely verified by growth rate, morphology, and/or flow cytometry and verified to be mycoplasma-free before experiments.

METHOD DETAILS

Tumor-on-chip concept, design and fabrication

The tumor-on-chip consists of two stacked microfluidic channels separated by an isoporous, semipermeable polyethylene terephthalate (PET) membrane (5 μ m poresize: $r_P = 5 \mu$ m; $\rho_P = 6 \times 10^5$ pores per cm²; TRAKETCH PET 5.0 p S210 \times 300, SABEU GmbH & Co. KG, Northeim, Germany), which was functionalized by a plasma-enhanced, chemical vapor deposition (PECVD) process as previously described. The tumor chambers (1 mm in diameter, 0.3 mm in height, six chambers per chip) branch off a main injection channel (0.2 mm in height) at a 45° angle and a high-resistance channel towards the outlet port, which forces the aggregates/organoids to sequentially enter the tumor chambers during the injection process, utilizing an injection mechanism previously successfully established in other organ-on-chip model. This concept and design enable the integration of any aggregate/organoid below 0.2 mm in size. The tumor channel is designed to have an outlet channel that possesses a fluidic resistance of 1.2 x 10¹² Pa.s/m³, which is at least twice higher than the fluidic resistance of the membrane and the medium channel combined. This ensures the placement of the cells into the tumor chambers during the injection instead of flowing out toward the outlet. The medium channel is situated right above the tumor chambers and is separated by a porous PET membrane that serves multiple functions: during the cell injection step, it enables the entrapment of the tumor aggregates/PDOs and provides a growth surface for the endothelial barrier formation, whereas during the culture period, its 5 μ m pore size allows T cell trafficking and passive diffusion of diluted species. In the place of the injection of diluted species.

The tumor and medium layers consisting 200-300 µm high channels were microstructured via replica molding of polydimethylsiloxane (PDMS; Sylgard 184, Dow Corning, USA) on two differently patterned master wafers fabricated via photolithographic processes. 55 The SU-8 structures on the tumor layer wafer have two heights: 300 µm for the round tumor chambers and 200 µm for the rest of the channels. For the replica molding, PDMS was homogeneously mixed in a 10:1 (elastomer base:curing agent) mass ratio and then degassed in a desiccator to remove air bubbles. Afterwards, two different replica molding approaches were conducted as previously described. 11 Standard molding approach was used by pouring the PDMS prepolymer solution onto the silicon wafer master mold to obtain 3 mm thick PDMS pieces with channel structures for the medium layer. PDMS was cured at 60 °C for 4 h. After curing, the PDMS were cut to the size of the chip and ports were pierced using a biopsy punch (Disposable Biopsy Punch, 0.75 mm diameter; 504 529; World Precision Instruments, Friedberg, Germany) to access the chips (for both cell injection and medium perfusion). The exclusion molding approach was used to fabricate the bottom tumor layer: here, PDMS prepolymer solution was poured onto the silicon wafer master mold, which was then clamped against a 5 mm-thick PMMA disk to produce a 0.3 mm thin layer with through hole channel structures. PDMS was cured at 60 °C for 2 h. Once the PDMS parts were cured, they were cleaned using isopropanol followed by deionized water and blow-dried with nitrogen pistol. The microfluidic chips were assembled in three consecutive bonding steps: (i) tumor layer to glass coverslip, (ii) medium layer to the membrane, (ii), and (iii) the tumor layer to medium layer. In all steps, bonding was achieved by oxygen plasma activation (75 W, 0.2 cm³m-1 O₂; Diener Zepto, Diener electronic GmbH + Co. KG, Ebhausen, Germany) for 24 s. Bonded parts were baked at 60 °C for at least 30 min after each bonding step, and overnight after the entire chip was assembled. All chips were O₂-plasma treated (75 W, 0.2 cm³m-1 O₂) for 5 min to sterilize and hydrophilize the PDMS surface before cell injection.

Tumor and fibroblast aggregates generation

Aggregates were formed using agarose microwells-based approach. 56 Briefly, 2.5 g of Hydrosil silicone components (1:1 wt) (101301; SILADENT) was added into each well of 6-well microwell culture plate (AggreWell400; STEMCELL Technologies) followed by centrifugation at 55 x g for 1 min and curing at 60 °C for 1 h. The cured molds were then carefully removed, cut into circular segments (d = 20 mm), and glued to a polymethyl methacrylate (PMMA) holder that has circular cutouts that match the surface of a 24-well plate (d = 15.5 mm, h = 2 mm). These cured molds were used as a reusable master mold for the agarose gel.

Prior to aggregate formation, the master molds were disinfected with 70% (v/v) ethanol and rinsed three times with PBS without Ca and Mg (indicated as PBS $^-$ in the following) (P04-36500; PAN-Biotech). Afterwards, 3% (w/v) agarose solution in DMEM (41965039; Gibco) was liquified by preheating in a microwave and 650 μ L was added into each master mold and left for 10 min at room temperature (RT) to allow agarose gelation. Afterwards, the agarose molds were transferred into the wells of 24-well plate with the patterned



structures facing upwards. The wells were filled with 1 mL of PBS⁻ followed by centrifugation at 1300 x g for 3 min to remove trapped air bubble below the agarose mold. PBS⁻ was removed before adding the cells.

To generate the MDA-MB-231 aggregates, the cells were detached by incubation for 3 min with TrypLE Express Enzyme (12604013; Gibco) at 37 $^{\circ}$ C, pelleted by centrifugation at 200 x g for 5 min and resuspended in RPMI-1640-based cell culture medium described above. The cell suspension was then mixed with basement membrane extract (BME) (Cultrex Reduced Growth Factor Basement Membrane Extract, Type 2 Select, 3533-005-02; Bio-techne) in 1:1 (v/v) ratio on ice and pipetted into each agarose well with 200 μ L mixture solution containing 100,000 cells. The 24-well plate was immediately centrifuged at 4 $^{\circ}$ C at 900 x g for 10 min, followed incubation for 30 min at 37 $^{\circ}$ C, 5% CO₂ and 95% rH for BME gelation. Afterwards, each well was supplemented with 1 mL of cell culture medium for 3 days of culture until chip injection.

To generate the fibroblast aggregates, a similar approach as described above was followed: fibroblasts were detached using TrypLE Express Enzyme for 3 min at 37 °C, pelleted by centrifugation at 200 x g for 5 min and resuspended in cell culture medium. 100,000 cells in 1 mL medium were pipetted into each agarose well. The 24-well plate was then centrifuged at RT at $900 \times g$ for $10 \times g$ f

Patient-derived tumor organoids generation and culture

Pleural effusion (PE) samples from four metastatic breast cancer patients were collected by thoracentesis and processed as followed. PE samples were centrifuged at 500 x g for 10 min. Cell pellets were pooled and when necessary, red blood cells were lysed with 10 mL of RBC lysis buffer (155 mM NH₄Cl, 10 mM KHCO₃, 100 μM Na2EDTA in H₂O, pH 7.4) on ice for 5 min. Cells were diluted in DPBS (Dulbecco's Phosphate Buffered Saline, P04-36500; Pan Biotech GmbH) and centrifuged at 500 x g for 10 min. The final cell pellet was resuspended in AdvDMEM/F12+++ (Advanced DMEM/F-12 (12534010), 1% Pen/Strep (15140122), 1x GlutaMAX (35050-038), 10 mM HEPES (15630-056); all from Thermo Fisher). For patient-derived organoid (PDO) culture setup, the desired amount of cell suspension was mixed with Basement Membrane Extract (BME; Cultrex Reduced Growth Factor Basement Membrane Extract, Type 2 Select, Bio-techne, 3533-005-02) at a ratio of 30% cell suspension to 70% BME. 20 μL droplets were plated into wells of a 48-well plate and placed upside-down in an incubator (37°C, 5% CO₂) to solidify for 30 min. Afterwards, 280 μL of culture medium (AdvDMEM/F12+++ supplemented with 10% (v/v) conditioned medium from L-WRN cells (ATCC-CRL-3276), 57 5 nM Heregulinβ-1 (100-03; PeproTech, NJ, USA), 5 ng/mL fibroblast growth factor 7 (FGF7) (100-19; PeproTech), 20 ng/mL fibroblast growth factor 10 (FGF10) (100-26; PeproTech), 5 ng/mL epidermal growth factor (EGF) (AF-100-15; PeproTech), 500 nM A83-01 (2939; Tocris, Wiesbaden, Germany), 5 μM Y27632 (72034; STEMCELL Technologies), 500 nM SB-202190 (S7067; Sigma-Aldrich), 2% B27 Supplement (17504-044; Thermo Fisher Scientific), 1.25 mM N-acetyl-cysteine (A9165; Sigma-Aldrich), 5 mM nicotinamide (N0636; Sigma-Aldrich)) was added to each well. The medium was changed every 3–4 days.

The PDOs were passaged based on the confluency of the culture, ranging from 5-20 days. PDOs were recovered from the wells by resuspending the BME-droplets in ice-cold DPBS containing 5 μ M Y-27632 (DPBS/Y-27632). This organoid suspension was incubated with 1 mL of TrypLE Express Enzyme (1X; Thermo Fisher, 12604013) at 37°C in a water bath for 5 min, followed by mechanical dissociation via 5 times pulling and dispensing the solution using a syringe with 27G needle (302200; Becton Dickinson). The suspension was then centrifuged at 500 x g for 10 min and the supernatant removed. For further culture, the desired amount of cell pellet was resuspended in AdvDMEM/F12+++ and mixed with BME at a ratio of 30% cell suspension to 70% BME and cultured as described above.

Prior to chip injection, the PDOs were expanded in a droplet of basement membrane extract hydrogel until they reached \sim 120 μ m in diameter, typically after \sim 10 days. To anticipate patient-specific differences in growth speed, the PDOs culture was monitored daily to better estimate the appropriate loading day. To retrieve the PDOs, gel droplets were first washed with PBS⁻ before introducing 500 μ L of 2 mg/mL cold dispase II solution followed by pipetting up and down to break the gel droplet. The organoid cell suspension was then incubated for 10 min at 37 °C, 5% CO₂ and 95% rH. Afterwards, each well was resuspended with 500 μ L of AdvD-MEM/F-12+++ and the retrieved PDOs were centrifuged at 500 x g for 5 min. Each droplet of PDOs on day 10 of culture was used to load 3 chips. After pelleting the PDOs, they were incubated in 10 μ M of CellTracker CMFDA solution (dissolved in phenol red-free DMEM/F-12 medium) for 20 min at 37°C, 5% CO₂ and 95% rH. The organoids were then washed twice by adding phenol red-free DMEM/F-12 medium up to 10 mL and centrifuged at 500 x g for 5 min for each washing cycle. The organoid pellet was then resuspended in dextran-based hydrogel as will be described in the next section.

Microvascular endothelial cells isolation and culture

From resected skin tissue from plastic surgeries, subcutaneous fat, visible blood vessels, and connective tissue were removed, and the remaining skin tissues were cut into strips of \sim 4 cm length and \sim 1 mm width, followed by incubation in 10 mL of 2 U/mL dispase solution (D4693; Merck KGaA) at 4 °C overnight. Next, the epidermis layer was peeled off and discarded, and the remaining dermis layer was washed twice in PBS $^{-}$. The mvECs were isolated from the dermis by incubating the dermis strips in 0.05% trypsin/EDTA (59417C; Sigma) for 40 min at 37 °C, followed by stopping the trypsinization with cell culture medium supplemented with 10% FCS and transferring the strips into a petri dish containing pre-warmed PBS $^{-}$. Next, the dissociated cells were scraped out with a scalpel and the cell suspension was strained through a 70 μ m strainer (542070; Greiner Bio-One) and collected. The cell suspension was then centrifuged at 209 x g for 5 min. Lastly, the cell pellet was resuspended in 10 mL of Endothelial Cell Growth Medium (ECGM, C-22010; PromoCell GmbH) supplemented with 10 mg/mL Gentamicin (15710049; Thermo Fisher Scientific). The cells were seeded



into two T25 cell culture flasks (690175; Greiner Bio-One) and incubated at 37 $^{\circ}$ C, 5% CO₂ and 95% rH. The cells were further expanded in T75 (658175; Greiner Bio-One) and used in passage 2 or 3 for this study.

Human induced pluripotent stem cells generation from PBMCs

HiPSCs were routinely cultured on Vitronectin XF in TeSR-E8 (all from Stem Cell Technologies) according to the manufacturer's protocol. Standard characterization of hiPSCs was performed as described previously. 58-60 Pluripotency of the hiPSC clones was confirmed by flow cytometry analysis for OCT3/4, SSEA-4, NANOG and spontaneous differentiation towards three germ lineages. G-banding analysis was conducted at the Laboratorium voor Diagnostische Genoomanalyse (LGDA), LUMC according to standard procedures. A total of 20 metaphases were analyzed for each line. Cell line authentication was performed by the Department of Human Genetics, LUMC, by using the PowerPlex Fusion System 5C autosomal STR kit (Promega) as previously described. Both clones from two hiPSC lines had normal karyotypes, showed expression of pluripotency markers and underwent tri-lineage differentiation (data not shown). Endothelial cells were generated (see below) from the following clones (donor-matched for both patients) and used in subsequent experiments: LUMC0228iCTRL03 p11 and LUMC0229iCTRL01 p11.

Human induced pluripotent stem cells-derived endothelial cells generation and culture

Endothelial cells were differentiated from hiPSCs through mesoderm specification under defined culture conditions followed by cryopreservation until chip culture, as previously described. ⁶² Cryopreserved hiPSC-derived endothelial cells were thawed in a water bath at 37 °C and transferred into a 15 mL tube containing 7 mL of Human Endothelial SFM medium (11111044; Thermo Fisher Scientific). The cells were centrifuged at 300 x g for 3 min and the pellet was resuspended in Human Endothelial SFM complete medium: Human Endothelial SFM medium supplemented with 20 ng/mL bFGF (130-093-564; Miltenyi Biotech), 30 ng/mL VEGF (130-109-396; Miltenyi Biotech), and 1% (v/v) human serum from platelet poor plasma (P2918; Sigma-Aldrich) and seeded into a T75 cell culture flask that was previously coated with 0.1% (w/v) gelatine solution for 1 h at 37 °C. The cells were expanded for 3-4 days prior to seeding into the tumor-on-chip and used only at passage 1.

Generation and culture of ROR1- and CD19-specific CAR-T cells

PBMCs were isolated by density gradient centrifugation from leukocyte apheresis of two different healthy donors using a separating solution with a density of 1.077 g/mL (Pancoll human; PAN Biotech). All donors provided their written informed consent.

CD4⁺ and CD8⁺ T cells were then isolated from PBMCs by magnetic associated cell sorting (MACS) using the CD4⁺ or CD8⁺ human T cell isolation kit (130-096-533 or 130-096-495; Miltenyi Biotec), respectively. Purity of isolated T cell fractions was verified by staining with fluorophore-conjugated antibodies (all from Biolegend, San Diego, CA, USA) and 7-AAD staining solution (130-111-568; Miltenyi Biotec) for dead cell exclusion on a MACS Quant 10 analyzer (Miltenyi Biotec). The following antibodies were used: anti-human CD3 PE (clone UCHT1), anti-human CD4 APC (clone RPA-T4), anti-human CD8 FITC (clone SK1).

T cells were seeded in 48-well plates (Costar plates; Corning) in CTL medium (RPMI 1640 supplemented with 1% (v/v) Penicillin/ Streptomycin, 1X GlutaMAX-I, 0.1% (v/v) 2-Mercaptoethanol [all from Thermo Fisher Scientific, Darmstadt, Germany] and 10% (v/v) pooled human serum [Bavarian Red Cross Center, Wiesentheid, Germany]) and activated using Dynabeads Human T-Activator CD3/ CD28 Beads and 50 U/mL rhIL-2 (Miltenyi Biotec).

The next day (day 1), two thirds of the medium was removed from all wells and T cells were treated with 5 ng/mL polybrene (Merck, Darmstadt, Germany). Lentiviral particles (MOI=3) encoding the ROR1 CAR construct (ROR1_41BB_CD3zeta_EGFRt)⁶³ or CD19 CAR construct (CD19_41BB_CD3zeta_EGFRt) were added to the cells (untransduced control: polybrene only) and centrifuged at 800 x g for 45 minutes at 32 °C. Afterwards, cells were incubated for 4 h at 37 °C, 5% CO₂ and 95% rH. Then, CTL medium supplemented with 50 U/mL rhIL-2 was added to all wells and cells were fed every other day by removing half of the medium from each well and adding CTL supplemented with 100 U/mL rhlL-2 (final conc. 50 U/mL rhlL-2). On day 7, CD3/CD28 Beads were magnetically removed and transduction efficacy was analyzed by staining with fluorophore-conjugated antibodies (all from Biolegend) and 7-AAD staining solution (Miltenyi Biotec) for dead cell exclusion on a MACS Quant 10 analyzer (Miltenyi Biotec). The following antibodies were used: anti-human EGFR Alexa Fluor 488 (clone AY13), anti-human CD4 APC (clone RPA T4), anti-human CD8 Pacific Blue (clone SK1). On day 9, CAR-modified (that is, EGFRt-positive) T cells were enriched by MACS using an in-house biotinylated anti-EGFR antibody (Cetuximab, Eli Lilly and Company, Indianapolis, IN, USA) and anti-Biotin Microbeads (Miltenyi Biotec). Purity of enriched CAR modified T cells was analyzed as described above. On the following day, enriched CAR modified as well as untransduced T cells were subjected either to an antigen-independent expansion protocol using irradiated CD19+ feeder cells as well as irradiated third-party donor PBMCs (ROR1-specific CAR-T cells) or to an antigen-dependent expansion protocol using irradiated CD19⁺ feeder cells (CD19-specific CAR-T cells). 14 days later, purity of expanded CAR-modified T cells was analyzed as above. Then, cells were counted using a Countess Counting II FL Device (Thermo Fisher Scientific) and cryopreserved at 10 million cells/ mL in Cryo SFM freezing medium (C-29910; PromoCell GmbH).

Three days before the perfusion through the chips, each subset (i.e. CD4 and CD8) of cryopreserved control T and CAR-T cells were thawed, centrifuged at 300 x g for 8 min at 8 °C, counted and seeded in 24-well cell culture plates at a concentration of 3.0 x 10⁶ cells per well. T cells were cultured for 3 days in X-VIVO 15 medium (BE02-060F; Lonza) supplemented with 5 ng/mL of rhIL-15 (130-093-955; Miltenyi Biotec), 1X Glutamax and 100 U/mL penicillin-streptomycin.





Aggregates/spheroids/PDOs seeding on-chip

After chips sterilization and hydrophilization with O_2 -plasma, the channels are flushed using 100 μ L pipette with 70% ethanol followed by rinsing three times with PBS $^-$. The chips were kept at RT until cell seeding. The cells were seeded into the chip at two to four days before T cells perfusion.

To retrieve the MDA-MB-231 aggregates from the plate, cell culture medium was firstly removed from the wells before introducing $500~\mu L$ of 2 mg/mL cold dispase II solution followed by pipetting up and down to break the gel. The plate was then incubated for 10~min at 37~C, $5\%~CO_2$ and 95%~rH. For the fibroblast spheroids, this gel digestion step was skipped as no gel was used for the spheroids generation. Afterwards, each well was resuspended with 1~mL of cell culture medium and the retrieved aggregates/spheroids were centrifuged down at 500~x g for 5~min. The pellet was then resuspended in dextran hydrogel (3-D Life Dextran-CD Hydrogel SG; Cellendes GmbH) supplemented with RGD peptide (09-P-001; Cellendes GmbH) with a final concentration of 0.5~mmol/L. Aggregates/spheroids from one well were used to load 3~chips.

To retrieve the PDOs from the plate, gel droplets were first washed with PBS⁻ before introducing 250 μ L of 2 mg/mL cold dispase II solution followed by pipetting up and down to break the gel droplet. The PDO suspension was then incubated for 10 min at 37 °C, 5% CO₂ and 95% rH. Afterwards, each well was resuspended with 500 μ L of advDMEM/F-12 +/+/+ and the retrieved PDOs were centrifuged down at 500 x g for 5 min. The pellet was resuspended in dextran hydrogel supplemented with 0.5 mmol/L RGD peptide. Each droplet of PDOs on day 10 of culture was used to load 3 chips.

In experiments that required PDOs/spheroids fluorescence-labeling, PDOs/spheroids pellet was resuspended in 10 μ M of CellTracker CMFDA dye solution (C7025; Invitrogen) dissolved in phenol red-free DMEM/F-12 medium and incubated for 20 min at 37 °C, 5% CO₂ and 95% rH. The cells were then washed twice by adding phenol red-free DMEM/F-12 medium up to 10 mL and centrifuging at 500 x g for 5 min for each washing cycle. Afterwards, the pellet was resuspended in dextran hydrogel supplemented with 0.5 mmol/L RGD peptide.

Once the cells were suspended in the hydrogel, 10 μ L was immediately injected into each chip via the tumor inlet. In the "empty chip" condition, blank hydrogel was injected without cells. Afterwards, the inlet and outlet of the medium channel were plugged using a metal wire with 0.7 mm diameter (45473; Menzanium) and the main tumor channel was flushed via negative pressure to remove any remaining cells. Then, plugs from the medium channel inlet and outlet were carefully removed and inserted into the tumor channel inlet and outlet. The medium channel was subsequently flushed three times with 100 μ L of cell-specific culture medium to remove any deposited hydrogel that might disrupt the subsequent endothelial cells attachment and fluidic flow. The chips were then incubated at 37 °C, 5% CO₂ and 95% rH for 30 min to allow hydrogel crosslinking.

Endothelial cells seeding, chip culture, and characterization

MvECs were harvested by first removing the cell culture medium from the flask, rinsing with PBS $^{-}$, followed by the insertion of 2 mL TrypLE Select (12563-029; Gibco). The flask was incubated for 3 min at 37 $^{\circ}$ C, 5% CO $_{2}$ and 95% rH to detach the cells. The trypsinization was stopped by adding 200 μ L of FCS into the solution, followed by transferring the solution into 15 mL tube. The cells were centrifuged at 200 x g for 5 min and resuspended in ECGM to achieve 9 x 10 6 cells/mL concentration for chip seeding. In case of hiPSC-ECs, the cells were harvested in a similar way with minor differences: the trypsinization process was done for 5 min at RT, and the cells were lastly centrifuged at 300 x g for 3 min at RT.

Endothelial cells were seeded into the chip on the same day of tumor cell loading and after the hydrogel in the tumor chambers was crosslinked. First, the medium channel of each chip was coated with 100 μ L solution containing 100 μ g/mL collagen-I (FibriCoI, #5133; Advanced Biomatrix) and 20 μ g/mL fibronectin (#F1141; Sigma Aldrich) for 1 h at 37 °C, 5% CO₂ and 95% rH. The medium channel was then flushed three times with ECGM. Afterwards, 5 μ L of cell suspension (concentration 9 x 10⁶ cells/mL) was injected into the medium channel inlet, followed by incubation for 4 h at 37 °C, 5% CO₂ and 95% rH to allow cell attachment on the membrane. Filter pipet tips filled with 100 μ L ECGM each were added into the inlet and outlet of the medium channel for 24 h of static culture. The chips were cultured for 4 days in push mode until control T and CAR-T cells perfusion. This culture duration was shortened to 1-2 days in some cases if stable endothelium was observed earlier. The details of the perfusion setup are described in the section below. Prior to the T cell perfusion, random chip samples were picked for immunofluorescence staining of the CD31 expression. Briefly, CD31 antibody (anti-human, APC, REAfinity; 130-110-808; Miltenyi Biotec) [in 1:35 working concentration] and Hoechst 33342 [in 1:250 working concentration] were diluted in ECGM. 50 μ L of the solution was gently introduced into the chip's medium channel followed by incubation for 30 min at 37 °C, 5% CO₂ and 95% rH. The staining solution was rinsed gently three times with ECGM before image acquisition.

For terminal immunofluorescence staining, cells were fixed by introducing ROTIHistofix 4% (P087.1; Carl Roth) into the chip's medium channel and incubated for 30 min at RT. Subsequently, the chip's medium channel was washed with PBS¯ and blocking solution (3% BSA in PBS¯) was incubated for another 30 min at RT. The primary antibody solution was prepared by diluting CD31 (anti-human, M0823; DAKO) and VE-Cadherin (anti-human, 36-1990; Invitrogen) 1:50 in antibody diluent (S0809; DAKO). This solution was incubated in the chip's medium channel overnight at 4 °C. On the next day, the primary antibody solution was replaced by PBS¯ and unspecificly bound antibodies were washed off by rinsing the medium channel twice with PBS¯. The secondary antibody solution was obtained by diluting the antibodies (Goat anti-Rabbit IgG (Heavy chain), Superclonal Recombinant Secondary Antibody, Alexa Fluor 555 and Goat anti-Mouse IgG (H+L), Superclonal Recombinant Secondary Antibody, Alexa Fluor 647) 1:100 in DAKO antibody diluent and adding DAPI [1 µg/mL working concentration]. This solution was incubated in the chip's medium channel for 1 h at RT. Chips were washed twice with PBS¯ prior to imaging. Thorough characterization of the endothelium has been performed in our previous studies employing the same seeding and culture method. ^{10,11}



For the barrier permeability assay, 4 kDa FITC- and 40 kDa-TRITC dextran were perfused through the medium channel either through chips containing mvEC barrier and MDA-MB-231 aggregates or blank chips. Fluorescence intensity was measured in the tumor tissue channel and normalized to the maximum fluorescence intensity in the medium channel. Images were taken every 3.7 min for up to 2 h using an epifluorescence microscope (Axio Observer 7, Carl Zeiss). The microscope chamber temperature was set to 37 °C during the acquisitions.

T cell perfusion and chip culture

To prepare the T cells, each subset (CD4 and CD8) of the cultured control T and CAR-T cells were retrieved from the 24-well plate and pipetted through a 70 μ L strainer to filter out cell clumps. Cells were centrifuged at 300 x g for 8 min at 8 °C followed by cell counting. To mimic the CAR-T cell product formulation in clinical trials, the typical 1:1 CD4+/CD8+ T cell ratio was selected throughout our experiments, 14,15 as it has shown a superior antitumor reactivity in an in vivo study and their cooperation is essential to exert potent and long-lasting antitumor activity. 64-66 Prior to the perfusion, both subsets were mixed and the concentration was set to 0.5 x 106 cells/mL. The concentration was set to 100,000 cells/mL and 1,000,000 cells/mL only in preliminary experiments to determine the optimal perfused T cell concentration (Figure S1E). In experiments that required fluorescence-labeling of T cells, T cell pellet was resuspended in 2 μ M of CellTracker Deep Red dye solution (C34565; Invitrogen) dissolved in phenol red- and serum-free DMEM/F-12 medium and incubated for 15 min at 37 °C, 5% CO₂ and 95% rH. The cells were then washed twice by adding fully supplemented X-VIVO 15 medium up to 10 mL and centrifuging at 300 x g for 8 min at 8 °C for each washing cycle. Afterwards, the final cell pellet was resuspended in ECGM basal medium (C-22210; PromoCell GmbH) supplemented with 2% FCS, 12 μ g/mL ECGS, 90 μ g/mL heparin, 0.1 ng/mL EGF, 1 ng/mL bFGF (all from the Growth Medium SupplementPack C-39210; PromoCell GmbH) – this will be referred to as "coculture medium" in the following.

Day of control T and CAR-T cell perfusion was defined as day 0 for all experiments. Starting from day 0, the chips were connected to constant medium perfusion via an external syringe pumping system (LA-190, Landgraf Laborsysteme HLL GmbH, Langenhagen, Germany). The chips were connected to the syringe pump using blunt 21 GA stainless steel needles (made from the dispensing needles by removing the plastic hub after dissolving the glue overnight in a 70% ethanol solution) connected to Tygon tubings (0.51 mm inner diameter, Tygon ND 100-80 Medical Tubing, Saint-Gobain Performance Plastics Pampus GmbH, Willich, Germany), 21 GA stainless steel plastic hub dispensing needles (e.g., KDS2112P, Weller Tools GmbH, Besigheim, Germany) and Luer Lock style syringes. For (CAR-)T cell perfusion through the medium channel, the inlet of the channel was equipped with a 100 µL-pipette tip reservoir holding the 400 μ L of T cell suspension (200,000 T cells/chip). The syringe pump was set to the withdraw mode at 100 μ L/h to ensure steady flow before introducing the (CAR-)T cells, thereby preventing them to precipitate on the inlet area. Once the (CAR-)T cells were suspended in the pipette tip reservoir, the flow rate was set to 20 µL/h and the whole setup was transferred into an incubator at 37 °C, 5% CO₂ and 95% rH. After 20 h, the chip effluents and plate control supernatants were collected for further analysis and the perfusion setup was changed to push mode where coculture medium was dispensed from the syringes. The chips further linearly perfused in this mode at 20 µL/h flow rate until up to day 8. Medium in the syringes was refilled after 3 days of perfusion. Before chip perfusion, medium is warmed-up to 37 °C and simultaneously degassed (vacuum source -70 kPa) and filter-sterilized using a Steriflip conical filter unit for 20 min. Effluent samples from each chip were collected every one or two days, centrifuged at 200 x g for 5 min to remove perfused cells, then at 10,000 x g for 10 min to remove debris and stored at -80 °C until further analysis. Terminal dead cell staining was done by introducing 20 $\mu g/mL$ propidium iodide (P4170; Sigma Aldrich) solution into the media channel following lowed by static incubation of the chips for 5 min at 37 °C. The medium channels were rinsed three times with PBS before image acquisition.

For plate assay controls, the same amount of tumor aggregate per chip were plated into each well (48-well plate format), followed by the addition of 400 μ L of T cell suspension (200,000 control T or CAR-T cells (1:1 ratio of CD8⁺ and CD4⁺) per well). Cells were cocultured overnight in coculture medium. Supernatants from day 1 were collected, centrifuged the same way as the chip samples and stored at -80 °C until cytokine analysis (see "cytokine quantification assay" method section).

Dasatinib treatment

To model CRS intervention, dasatinib (S1021; Selleckchem) with a final concentration of 50 nM was supplemented in the coculture medium and perfused through the medium channel of the chips either from day 0-1, 0-8, or 1-8. This concentration was found to be potent to render CD19-CAR-T cells temporarily inactive. ¹² In a preliminary experiment, CAR-T cells were cultured either with or without MDA-MB-231 cells (effector-to-target cell ratio, 10:1) for 24 h, with or without dasatinib supplementation (50 nM final concentration) in the coculture medium. In the coculture condition, MDA-MB-231 cells were seeded as a monolayer and CAR-T cells (1:1 ratio of CD8⁺ and CD4⁺) suspension was added into the well. CAR-T cells were collected on the next day for flow cytometry staining with anti-human CD69 (early activation marker), anti-human CD25 (late activation marker). Viability was assessed also during flow cytometry by adding Zombie aqua dye (423102; BioLegend) into the staining solution (see "flow cytometry staining and analysis" method section).

Allogeneic / isogenic endothelial cells - (CAR-)T cells coculture for cytokine assay

To demonstrate the differences of allogeneic and isogenic setup in terms of cytokine release by the T cells, we selected five mvECs donors for 24 h coculture with T cells. HiPSC-ECs was used in the isogenic setup. Briefly, endothelial cells were plated (10,000 cells/well, 96-well plate format) and cultured overnight. On the next day, 200,000 control T or CAR-T cells (1:1 ratio of CD8⁺ and CD4⁺) were





added into each well (effector-to-target cell ratio, 20:1). Cells were cocultured overnight and coculture medium was used: see method section "T cell perfusion and chip culture" for the composition. Supernatants were collected and stored at -80 °C until cyto-kine analysis (see "cytokine quantification assay" method section).

QUANTIFICATION AND STATISTICAL ANALYSIS

Image acquisition and analysis

For the timepoint live imaging of T cell infiltration, GFP fluorescence intensity of the MDA-MB-231 tumor aggregates and tumor aggregate area, an epifluorescence microscope (Axio Observer 7, Carl Zeiss) was used and the focal plane was set to focus on the aggragate/spheroid/PDO. The microscope chamber temperature was set to 37 °C during all live cell imaging acquisitions of the chips. Analyses of T cell infiltration, GFP fluorescence intensity of the MDA-MB-231 tumor aggregates and tumor aggregate area were conducted using ImageJ-Fiji software. 52 For T cell intensity measurements, the histogram of the fluorescent images was adjusted to remove the background signal, followed by quantification of the mean gray value of the CellTracker Deep Redlabeled (CAR-)T cells within the region of interest (ROI) of each tumor aggregate/fibroblast spheroid/PDO. Tumor aggregates/fibroblasts spheroids/PDOs smaller than 50 µm in diameter were considered too small and therefore excluded from the analysis. Tumor aggregate/fibroblasts spheroid/PDO ROI was defined by automated thresholding of the GFP signal (for MDA-MB-231 aggregates) or the CellTracker CMFDA signal (for fibroblasts spheroids and PDOs). Area of MDA-MB-231 aggregates or PDOs was measured after thresholding to analyze their growth upon control T or CAR-T cell treatment, and aggregates/PDOs area from day > 0 was compared with their initial area before control T or CAR-T cell perfusion. For GFP fluorescence intensity analysis of the tumor aggregate, the mean gray value of tumor aggregates was measured and compared with their initial mean gray value on day 0. To guantify T cells in the whole tumor chamber or within the tumor aggregate, a spinning disk confocal microscope (Cell Observer Z1, Carl Zeiss) was used. Here, confocal z-stacks imaging data were used to run the Spot Detection function in Imaris 9.5 software (Oxford Instruments). The estimated XY and Z diameter of T cells was set to 5 µm and 10 µm, respectively. Tumor aggregate volume was rendered using the Surfaces function. The number of infiltrating (CAR-)T cells was quantified by counting the subset of (CAR-)T cells that have zero distance (colocalized) to the tumor aggregate. For all measurements, image data from a minimum of 3 chips were pooled for each condition for further statistical analysis. To measure MDA-MB-231 aggregates diameter after the aggregate generation method using the agarose microwells-based approach, a randomly selected area in the well (three wells in total) was imaged and further processed for automated thresholding and subsequent diameter measurement in ImageJ-Fiji to check for the diameter variability.

Cytokine quantification assay

Cytokines from undiluted samples from chips/plates were analyzed by fluorescent bead-based multiplex sandwich immunoassays (Legendplex Human CD8/NK Mix and Match Subpanel; BioLegend) containing capture beads targeting IL-2, IL-6, IL-10, TNF- α , IFN- γ and granzyme B and read by flow cytometry (BD LSR II or BD LSRFortessa, BD Biosciences) according to manufacturer's protocol. Flow cytometry data files were manually gated using LEGENDplex Cloud-Based Data Analysis Software Suite (BioLegend) to find the optimal differentiation between capture bead populations and subsequently applied to all datasets.

Flow cytometry staining and analysis

For the analysis of the expression of extracellular markers, the following antibodies were used depending on the experiment: anti-human ROR1 APC (130-118-015; Miltenyi Biotec), anti-human CD31 FITC (130-110-806; Miltenyi Biotec), anti-human CD3 PE/Cyanine7 (317334; BioLegend), anti-human CD4 APC/Fire750 (357426; BioLegend), anti-human CD8a PerCP (300922; BioLegend), anti-human CD69 FITC (310904; BioLegend) and anti-human CD25 BV421 (302630; BioLegend). Detailed information on the antibodies is summarized in the "key resources table". 96-well V-bottom cell culture plate was used for staining and flow cytometry reading. For staining, cells in each well were firstly washed with flow cytometry staining buffer: 3% FCS with 2 mM EDTA (15575020; Invitrogen) in PBS⁻. Cells were then incubated in a blocking solution containing Human BD Fc Block (564220; BD Biosciences) diluted 1:25 (v/v) in PBS⁻ for 15 min at 4 °C. Afterwards, cells were incubated for 30 min at 4° C in the antibody-mixture solution specific for each experiment. Zombie aqua dye (423102; BioLegend) was added 1:200 in the antibody-mixture solution to differentiate the viable cells during analysis. Cells were then washed twice with the staining buffer, fixed with ROTIHistofix 4% (P087.6; Carl Roth GmbH) for 10 min at RT, then washed and resuspended in the staining buffer. The samples were analyzed directly using flow cytometry (BD LSR II or BD LSRFortessa, BD Biosciences) or kept stored at 4 °C for maximum overnight until analysis. Autofluorescence and isotype controls were included in every staining procedure. For the analysis, FSC-A and SSC-A properties were used to identify cells, cell doublets were excluded based on FSC-H vs. FSC-A. Dead cells were excluded from analysis. Primary cancer cells, cancer cell lines and endothelial cells were analyzed with established ROR1 marker by using unstained cells as cut-off. Same strategy was applied for CD31 staining on hiPSC-derived endothelial cells. For T cell analyis, T cell subpopulations were gated according to established markers and analyzed for activation marker expression by comparing activation marker signal in untreated vs. treated T cells.

Statistics and reproducibility

In all experiments, every chip is considered an independent biological replicate. For each run of chips, the same condition was performed at least twice. For graphs with a statistical analysis, the minimum sample size is 3. The sample size criteria depended on the



logistical complexity of the whole experiment, primary and iPS cells availability, distribution of donors to assure paired conditions, availability of pumping systems and technical issues. The criteria was the following: for proof of concept data, the sample size of 2 is the minimum; for the following experiments, a minimum sample size is 4. Every test was performed in parallel with the respective control conditions. Chips were randomly allocated into experimental groups using a numbering system for distinguishing them, which was kept until analysis. Chips were excluded from the analysis if technical issues with the microfluidic setup occured (e.g. leakages, flow blockage due to bubbles). For the cytokine analysis, only chips with the correct effluent volume were considered. For the image analysis, aggregate/spheroid/organoid smaller than $50 \, \mu m$ in diameter were considered too small and therefore excluded from the downstream analysis. The number of biological replicates is described in each figure caption. For imaging-based quantification, n denotes the number of aggregates/spheroids/PDOs or tumor chambers, as indicated in each figure caption. For the effluent analysis, n denotes the number of chip replicates. Statistical analysis was performed using GraphPad Prism 9.2.0 software, and graphs are represented as average values \pm SEM unless indicated otherwise. Detailed statistics are indicated in each figure legend.